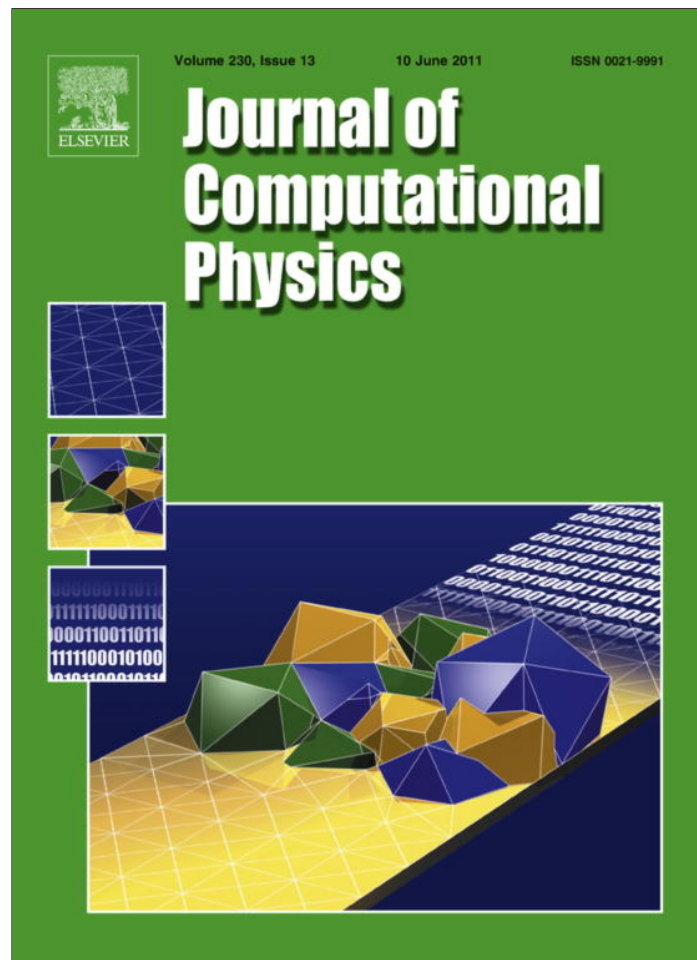


Provided for non-commercial research and education use.
Not for reproduction, distribution or commercial use.



This article appeared in a journal published by Elsevier. The attached copy is furnished to the author for internal non-commercial research and education use, including for instruction at the authors institution and sharing with colleagues.

Other uses, including reproduction and distribution, or selling or licensing copies, or posting to personal, institutional or third party websites are prohibited.

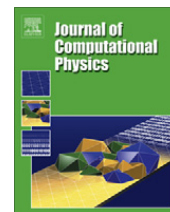
In most cases authors are permitted to post their version of the article (e.g. in Word or Tex form) to their personal website or institutional repository. Authors requiring further information regarding Elsevier's archiving and manuscript policies are encouraged to visit:

<http://www.elsevier.com/copyright>



Contents lists available at ScienceDirect

Journal of Computational Physics

journal homepage: www.elsevier.com/locate/jcp

Numerical methods for computing ground states and dynamics of nonlinear relativistic Hartree equation for boson stars

Weizhu Bao*, Xuanchun Dong

Department of Mathematics and Center for Computational Science and Engineering, National University of Singapore, Singapore 119076, Singapore

ARTICLE INFO

Article history:

Received 8 November 2010
 Received in revised form 22 March 2011
 Accepted 26 March 2011
 Available online 2 April 2011

Keywords:

Relativistic Hartree equation
 Boson stars
 Ground state
 Dynamics
 Backward Euler sine pseudospectral method
 Time-splitting sine pseudospectral method

ABSTRACT

Efficient and accurate numerical methods are presented for computing ground states and dynamics of the three-dimensional (3D) nonlinear relativistic Hartree equation both without and with an external potential. This equation was derived recently for describing the mean field dynamics of boson stars. In its numerics, due to the appearance of pseudodifferential operator which is defined in phase space via symbol, spectral method is more suitable for the discretization in space than other numerical methods such as finite difference method, etc. For computing ground states, a backward Euler sine pseudospectral (BESP) method is proposed based on a gradient flow with discrete normalization; and respectively, for computing dynamics, a time-splitting sine pseudospectral (TSSP) method is presented based on a splitting technique to decouple the nonlinearity. Both BESP and TSSP are efficient in computation via discrete sine transform, and are of spectral accuracy in spatial discretization. TSSP is of second-order accuracy in temporal discretization and conserves the normalization in discretized level. In addition, when the external potential and initial data for dynamics are spherically symmetric, the original 3D problem collapses to a quasi-1D problem, for which both BESP and TSSP methods are extended successfully with a proper change of variables. Finally, extensive numerical results are reported to demonstrate the spectral accuracy of the methods and to show very interesting and complicated phenomena in the mean field dynamics of boson stars.

© 2011 Elsevier Inc. All rights reserved.

1. Introduction

In this paper, we aim to design efficient and accurate numerical methods for computing ground states and dynamics of the three-dimensional (3D) nonlinear relativistic Hartree equation [17,27,28]:

$$i\partial_t\psi(\mathbf{x}, t) = \sqrt{-\Delta + m^2}\psi + V(\mathbf{x})\psi + \lambda(|\mathbf{x}|^{-1} * |\psi|^2)\psi, \quad \mathbf{x} \in \mathbb{R}^3, \quad t > 0, \quad (1.1)$$

with the following initial condition for dynamics

$$\psi(\mathbf{x}, 0) = \psi_0(\mathbf{x}), \quad \mathbf{x} \in \mathbb{R}^3. \quad (1.2)$$

Here, t is time, $\mathbf{x} = (x, y, z)^T$ is the Cartesian coordinates, $\psi = \psi(\mathbf{x}, t)$ is a complex-valued dimensionless wave function, a real-valued function $V(\mathbf{x})$ stands for an external potential, $m \geq 0$ denotes the scaled particle mass ($m = 1$ in most cases) with $m = 0$ corresponding to massless particles, and $\lambda \in \mathbb{R}$ is a dimensionless constant describing the interaction strength. The sign of λ

* Corresponding author.

E-mail addresses: bao@math.nus.edu.sg (W. Bao), dong.xuanchun@nus.edu.sg (X. Dong).

URL: <http://www.math.nus.edu.sg/~bao/> (W. Bao).

depends on the type of interaction: positive for the repulsive interaction and negative for the attractive interaction. The pseudodifferential operator $\sqrt{-\Delta + m^2}$ for the kinetic energy is defined via multiplication in the Fourier space with the symbol $\sqrt{|\xi|^2 + m^2}$ for $\xi \in \mathbb{R}^3$, which is frequently used in relativistic quantum mechanical models as a convenient replacement of the full (matrix-valued) Dirac operator [2,17,27,28]. The symbol $*$ stands for the convolution in \mathbb{R}^3 . In addition, the initial condition is usually normalized under the *normalization condition* by a proper non-dimensionalization

$$\|\psi_0\|^2 := \int_{\mathbb{R}^3} |\psi_0(\mathbf{x})|^2 d\mathbf{x} = 1. \tag{1.3}$$

The above nonlinear relativistic Hartree Eq. (1.1) was rigorously derived recently in [17] for a quantum mechanical system of N bosons with relativistic dispersion interacting through a gravitational attractive or repulsive Coulomb potential, which is often referred to as a boson star. In fact, by starting from the N -body Schrödinger equation and choosing the initial wave function to describe a condensate where the N bosons are all in the same one-particle state, in the mean field limit $N \rightarrow \infty$, the authors [17] proved that the time evolution of the one-particle density is governed by the nonlinear relativistic Hartree equation (under a proper non-dimensionalization), see also [19,20]. Also, we refer readers to [2,27,28] and references therein (with a slightly different dimensionless scaling in some cases) for other physical backgrounds of (1.1).

It is easy to show that the Eq. (1.1) admits two important conserved quantities [2,17,19,20], i.e. the *mass* of the system

$$N(\psi(\cdot, t)) := \|\psi(\cdot, t)\|^2 = \int_{\mathbb{R}^3} |\psi(\mathbf{x}, t)|^2 d\mathbf{x} \equiv \int_{\mathbb{R}^3} |\psi_0(\mathbf{x})|^2 d\mathbf{x} = 1, \quad t \geq 0 \tag{1.4}$$

and the *energy*

$$E(\psi(\cdot, t)) := \int_{\mathbb{R}^3} \left[\psi^* (-\Delta + m^2)^{1/2} \psi + \left(V(\mathbf{x}) + \frac{\lambda}{2|\mathbf{x}|} * |\psi|^2 \right) |\psi|^2 \right] d\mathbf{x} \equiv E(\psi_0), \quad t \geq 0, \tag{1.5}$$

where f^* denotes the complex conjugate of a function f .

The well-posedness of the initial-value problem (1.1)-(1.2) was extensively studied in [2,13,20,27] and references therein. Their results can be summarized as: (i) there exists a universal constant λ_{cr} (also referred to as the “Chandrasekhar limit mass” in physics [29] and with a lower bound $\lambda_{cr} > 4/\pi$) such that, when $\lambda > -\lambda_{cr}$, the solution is globally well-posed in the energy space $H^{1/2}(\mathbb{R}^3)$ provided that $V \in L^3(\mathbb{R}^3) \cap L^\infty(\mathbb{R}^3)$; (ii) when $\lambda \leq -\lambda_{cr}$, the solution is locally well-posed; and (iii) when $\lambda < -\lambda_{cr}$, the solution will blow up in finite time, which indicates the “gravitational collapse” of boson stars when the effective ‘mass’ exceeds the critical value λ_{cr} [20]. Another problem of interests is the existence and uniqueness of the ground state for (1.1), which is defined as the minimizer of the following nonconvex minimization problem:

Find $\phi_g \in S = \{\phi | \phi \in H^{1/2}(\mathbb{R}^3), \|\phi\|^2 = 1\}$ such that

$$E_g := E(\phi_g) = \min_{\phi \in S} E(\phi). \tag{1.6}$$

If $V(\mathbf{x}) \equiv 0$, it was shown that the ground state exists iff $-\lambda_{cr} < \lambda < 0$ [19,29] and any ground state is smooth, decays exponentially when $|\mathbf{x}| \rightarrow \infty$, and is identical to its spherically symmetric rearrangement up to phase and translation. Moreover, it was proven recently in [28] that, when $\lambda < 0$ and $|\lambda| \ll 1$, the spherical-symmetric ground state is unique up to phase and translation, and the author remarked there that whether such uniqueness result can be extended to the whole range of existence $-\lambda_{cr} < \lambda < 0$ remains open. Thus, such critical value λ_{cr} plays an important role in investigating the ground states and dynamics of (1.1). We remark here that based on our numerical results $\lambda_{cr} \approx 2.69 > 8/\pi$ (cf. Fig.2).

For Schrödinger–Poisson (or -Newton) equations, i.e. the pseudodifferential operator $\sqrt{-\Delta + m^2}$ in (1.1) is replaced by $-\Delta$ [10,23], different numerical methods were presented in the literatures based on finite difference discretization; see, e.g., [15,16,21,23]. However, these numerical methods have some difficulties in discretizing the 3D relativistic Hartree equation efficiently and accurately due to the appearance of the pseudodifferential operator. The main aim of this paper is to design efficient and accurate numerical methods for computing the ground state of (1.1) and the dynamics of the initial value problem (1.1)-(1.2). For this purpose, let $\beta = 4\pi\lambda$ and

$$\varphi(\mathbf{x}, t) = \frac{1}{4\pi|\mathbf{x}|} * |\psi|^2 = \frac{1}{4\pi} \int_{\mathbb{R}^3} \frac{1}{|\mathbf{x} - \mathbf{x}'|} |\psi(\mathbf{x}', t)|^2 d\mathbf{x}', \quad \mathbf{x} \in \mathbb{R}^3, \quad t \geq 0,$$

then (1.1) is re-written as the relativistic Schrödinger–Poisson (RSP) system

$$i\partial_t \psi(\mathbf{x}, t) = \sqrt{-\Delta + m^2} \psi + V(\mathbf{x})\psi + \beta\varphi\psi, \quad \mathbf{x} \in \mathbb{R}^3, \quad t > 0, \tag{1.7}$$

$$-\Delta\varphi = |\psi|^2, \quad \mathbf{x} \in \mathbb{R}^3, \quad \lim_{|\mathbf{x}| \rightarrow \infty} \varphi(\mathbf{x}, t) = 0, \quad t \geq 0. \tag{1.8}$$

With this formulation, the energy functional (1.5) is re-written as

$$\begin{aligned}
 E(\psi(\cdot, t)) &= \int_{\mathbb{R}^3} \left[\psi^*(-\Delta + m^2)^{1/2} \psi + \left(V(\mathbf{x}) + \frac{\beta}{2} \varphi \right) |\psi|^2 \right] d\mathbf{x} \\
 &= \int_{\mathbb{R}^3} \left[|(-\Delta + m^2)^{1/4} \psi|^2 + \left(V(\mathbf{x}) + \frac{\beta}{2} (-\Delta)^{-1} |\psi|^2 \right) |\psi|^2 \right] d\mathbf{x} \\
 &= \int_{\mathbb{R}^3} \left[|(-\Delta + m^2)^{1/4} \psi|^2 + V(\mathbf{x}) |\psi|^2 + \frac{\beta}{2} |\nabla \varphi|^2 \right] d\mathbf{x} \equiv E(\psi_0), \quad t \geq 0.
 \end{aligned} \tag{1.9}$$

In order to design numerical methods for computing the ground state, we first construct a gradient flow with discrete normalization (GFDN) which was widely and successfully used in computing ground states of Bose–Einstein condensation [5,3,21] and the Schrödinger–Poisson–Slater equations [36]. Then the problem is truncated into a box with homogeneous Dirichlet boundary conditions and a backward Euler sine pseudospectral method [4,3,36] is applied to discretize it. For computing the dynamics, again the problem is truncated into a box with homogeneous Dirichlet boundary conditions and a time-splitting sine pseudospectral method [6,7,9,3,36] is applied to discretize it. In particular, when the potential and initial data for dynamics are spherically symmetric, then the problem collapses to a quasi-1D problem. Simplified numerical methods are designed by using a proper change of variables in the quasi-1D problem.

The paper is organized as follows. In Section 2, a backward Euler sine pseudospectral method is proposed for computing the ground state in 3D. In Section 3, a time-splitting sine pseudospectral method is presented for computing the dynamics in 3D. In Section 4, simplified numerical methods are presented when the potential $V(\mathbf{x})$ and initial data $\psi_0(\mathbf{x})$ are spherically symmetric. Extensive numerical results are reported in Section 5 to demonstrate the efficiency and accuracy of our numerical methods and to show the ground states and mean field dynamics of boson stars. Finally, some closing remarks are drawn in Section 6. Throughout the paper, we adopt the standard Sobolev spaces and their corresponding norms.

2. Numerical method for computing ground state in 3D

In this section, we will propose an efficient and accurate numerical method for computing the ground state, i.e., solving the minimization problem (1.6). It is readily to verify that its Euler–Lagrange equation is:

$$\mu \phi(\mathbf{x}) = \sqrt{-\Delta + m^2} \phi(\mathbf{x}) + V(\mathbf{x}) \phi(\mathbf{x}) + \beta \varphi(\mathbf{x}) \phi(\mathbf{x}), \quad \mathbf{x} \in \mathbb{R}^3, \tag{2.1}$$

$$-\Delta \varphi(\mathbf{x}) = |\phi(\mathbf{x})|^2, \quad \mathbf{x} \in \mathbb{R}^3, \quad \lim_{|\mathbf{x}| \rightarrow \infty} \varphi(\mathbf{x}) = 0, \tag{2.2}$$

under the constraint

$$\|\phi\|^2 := \int_{\mathbb{R}^3} |\phi(\mathbf{x})|^2 d\mathbf{x} = 1, \tag{2.3}$$

where the eigenvalue μ is usually called as the chemical potential in physics literatures, which can be obtained by

$$\mu(\phi) = \int_{\mathbb{R}^3} \left[|(-\Delta + m^2)^{1/4} \phi|^2 + (V(\mathbf{x}) + \beta \varphi) |\phi|^2 \right] d\mathbf{x} = E(\phi) + \frac{\beta}{2} \int_{\mathbb{R}^3} \varphi |\phi|^2 d\mathbf{x}. \tag{2.4}$$

In fact, the above nonlinear eigenvalue problem can also be obtained by taking the ansatz

$$\psi(\mathbf{x}, t) = e^{-i\mu t} \phi(\mathbf{x}), \quad \mathbf{x} \in \mathbb{R}^3, \quad t \geq 0, \tag{2.5}$$

in (1.7)–(1.8). Thus it is also called as the time-independent relativistic Schrödinger–Poisson system.

2.1. Gradient flow with discrete normalization

In order to solve the nonconvex minimization problem (1.6) efficiently, we construct the gradient flow with discrete normalization (GFDN) following the procedure in [1,5,12]. Choose a time step $\Delta t > 0$ and set $t_n = n \Delta t$ for $n = 0, 1, \dots$. Applying the steepest decent method to the energy functional $E(\phi)$ in (1.5) without the constraint (2.3), and then projecting the solution back to the unit sphere S at the end of each time interval $[t_n, t_{n+1}]$ to enforce the constraint (2.3), we come to the following gradient flow with discrete normalization in 3D (GFDN-3D) for $\phi(\mathbf{x}, t)$:

$$\partial_t \phi = -\frac{1}{2} \frac{\delta E(\phi)}{\delta \phi} = -\sqrt{-\Delta + m^2} \phi - V(\mathbf{x}) \phi - \beta \varphi \phi, \quad \mathbf{x} \in \mathbb{R}^3, \quad t_n \leq t < t_{n+1}, \tag{2.6}$$

$$-\Delta \varphi = |\phi|^2, \quad \mathbf{x} \in \mathbb{R}^3, \quad \lim_{|\mathbf{x}| \rightarrow \infty} \varphi(\mathbf{x}, t) = 0, \quad t \geq 0, \tag{2.7}$$

$$\phi(\mathbf{x}, t_{n+1}) := \phi(\mathbf{x}, t_{n+1}^+) = \frac{\phi(\mathbf{x}, t_{n+1}^-)}{\|\phi(\mathbf{x}, t_{n+1}^-)\|}, \quad \mathbf{x} \in \mathbb{R}^3, \quad n \geq 0, \tag{2.8}$$

$$\phi(\mathbf{x}, 0) = \phi_0(\mathbf{x}), \quad \mathbf{x} \in \mathbb{R}^3, \quad \text{with} \quad \|\phi_0\|^2 = \int_{\mathbb{R}^3} |\phi_0(\mathbf{x})|^2 d\mathbf{x} = 1, \tag{2.9}$$

where $\phi(\mathbf{x}, t_n^\pm) := \lim_{t \rightarrow t_n^\pm} \phi(\mathbf{x}, t)$. In fact, the gradient flow (2.6) can also be obtained from (1.7) by setting time t to $\tau = i t$, thus the above construction is also referred to as the imaginary time method in physics literatures [5,14,26,32].

Letting $\Delta t \rightarrow 0$ in the GFDN-3D (2.6)–(2.9), similar as in [5,36], one can obtain the following continuous normalized gradient flow (CNGF):

$$\partial_t \phi(\mathbf{x}, t) = -\sqrt{-\Delta + m^2} \phi - V(\mathbf{x})\phi - \beta \phi \phi + \frac{\mu(\phi)}{\|\phi\|^2} \phi, \quad \mathbf{x} \in \mathbb{R}^3, \quad t > 0, \tag{2.10}$$

$$-\Delta \phi = |\phi|^2, \quad \mathbf{x} \in \mathbb{R}^3, \quad \lim_{|\mathbf{x}| \rightarrow \infty} \phi(\mathbf{x}, t) = 0, \quad t \geq 0. \tag{2.11}$$

It is easy to justify that the above CNGF is normalization conserved and energy diminishing, i.e.,

$$\|\phi(\mathbf{x}, t)\|^2 \equiv \|\phi_0\|^2 = 1, \quad \frac{d}{dt} E(\phi(\mathbf{x}, t)) = -2\|\phi_t(\mathbf{x}, t)\|^2 \leq 0, \quad t \geq 0.$$

Thus the positive ground state $\phi_g(\mathbf{x})$ can be obtained as the steady state solution of the GFDN-3D (2.6)–(2.9) or CNGF (2.10)–(2.11) with a positive initial data $\phi_0(\mathbf{x}) \geq 0$ for $\mathbf{x} \in \mathbb{R}^3$.

2.2. Full discretization in 3D

In practical computation, the whole space problem (2.6)–(2.9) is usually truncated into a bounded computation domain $\Omega = [a, b] \times [c, d] \times [e, f]$ for $|a|, b, |c|, d, |e|$ and f sufficiently large with homogeneous Dirichlet boundary conditions on $\partial\Omega$, i.e.

$$\partial_t \phi = -\sqrt{-\Delta + m^2} \phi - V(\mathbf{x})\phi - \beta \phi \phi, \quad \mathbf{x} \in \Omega, \quad t_n \leq t < t_{n+1}, \tag{2.12}$$

$$-\Delta \phi = |\phi|^2, \quad \mathbf{x} \in \Omega, \quad \phi(\mathbf{x}, t_{n+1}) := \phi(\mathbf{x}, t_{n+1}^+) = \frac{\phi(\mathbf{x}, t_{n+1}^-)}{\|\phi(\mathbf{x}, t_{n+1}^-)\|}, \quad n \geq 0, \tag{2.13}$$

$$\phi(\mathbf{x}, t)|_{\partial\Omega} = \varphi(\mathbf{x}, t)|_{\partial\Omega} = 0, \quad t \geq 0, \tag{2.14}$$

$$\phi(\mathbf{x}, 0) = \phi_0(\mathbf{x}), \quad \mathbf{x} \in \Omega, \quad \text{with} \quad \|\phi_0\|^2 = \int_{\Omega} |\phi_0(\mathbf{x})|^2 d\mathbf{x} = 1. \tag{2.15}$$

Let J, K, L be even positive integers and define the index sets,

$$\mathcal{T}_{JKL} = \{(j, k, l) : j = 1, 2, \dots, J-1, k = 1, 2, \dots, K-1, l = 1, 2, \dots, L-1\},$$

$$\mathcal{T}_{JKL}^0 = \{(j, k, l) : j = 0, 1, \dots, J, k = 0, 1, \dots, K, l = 0, 1, \dots, L\}.$$

Choose mesh sizes $h_x = (b-a)/J, h_y = (d-c)/K$ and $h_z = (f-e)/L$, let $h = \max\{h_x, h_y, h_z\}$, and define the grids

$$x_j = a + jh_x, \quad y_k = c + kh_y, \quad z_l = e + lh_z, \quad (j, k, l) \in \mathcal{T}_{JKL}^0.$$

Denote

$$Y_{JKL} = \text{span}\{\Phi_{pqs}(\mathbf{x}), \mathbf{x} \in \Omega, (p, q, s) \in \mathcal{T}_{JKL}\},$$

with

$$\Phi_{pqs}(\mathbf{x}) = \sin(\mu_p^x(x-a)) \sin(\mu_q^y(y-c)) \sin(\mu_s^z(z-e)), \quad \mathbf{x} \in \Omega, \quad (p, q, s) \in \mathcal{T}_{JKL},$$

$$\mu_p^x = \frac{\pi p}{b-a}, \quad \mu_q^y = \frac{\pi q}{d-c}, \quad \mu_s^z = \frac{\pi s}{f-e}, \quad (p, q, s) \in \mathcal{T}_{JKL}$$

and $\mathcal{P}_{JKL} : Y = \{U(\mathbf{x}) \in C(\Omega) : U(\mathbf{x})|_{\partial\Omega} = 0\} \rightarrow Y_{JKL}$ the standard projection operator [22,24,33], i.e.,

$$(\mathcal{P}_{JKL} U)(\mathbf{x}) = \sum_{(p,q,s) \in \mathcal{T}_{JKL}} \hat{U}_{pqs} \Phi_{pqs}(\mathbf{x}), \quad \mathbf{x} \in \Omega, \quad \forall U \in Y,$$

with \hat{U}_{pqs} the sine transform coefficients

$$\hat{U}_{pqs} = \frac{8}{(b-a)(d-c)(f-e)} \int_{\Omega} U(\mathbf{x}) \Phi_{pqs}(\mathbf{x}) d\mathbf{x}, \quad (p, q, s) \in \mathcal{T}_{JKL}. \tag{2.16}$$

Choosing $\phi^0(\mathbf{x}) = (\mathcal{P}_{JKL} \phi_0)(\mathbf{x})$, a backward Euler sine spectral discretization for (2.6)–(2.7) reads:

Find $\phi^{n+1}(\mathbf{x}) \in Y_{JKL}$ (i.e., $\phi^+(\mathbf{x}) \in Y_{JKL}$) and $\varphi^n(\mathbf{x}) \in Y_{JKL}$, such that,

$$\frac{\phi^+(\mathbf{x}) - \varphi^n(\mathbf{x})}{\Delta t} = -\sqrt{-\Delta + m^2} \phi^+(\mathbf{x}) - \mathcal{P}_{JKL}\{(V(\mathbf{x}) + \beta \varphi^n(\mathbf{x}))\phi^+(\mathbf{x})\}, \tag{2.17}$$

$$-\Delta \varphi^n(\mathbf{x}) = (\mathcal{P}_{JKL} |\phi^n|^2)(\mathbf{x}), \quad \phi^{n+1}(\mathbf{x}) = \frac{\phi^+(\mathbf{x})}{\|\phi^+(\mathbf{x})\|}, \quad \mathbf{x} \in \Omega, \quad n \geq 0. \tag{2.18}$$

The above discretization can be solved in phase space, but it is not suitable in practical computation due to the difficulty in evaluating the integrals in (2.16). Instead, we carry out an efficient implementation by choosing $\phi^0(\mathbf{x})$ as the interpolation of $\phi_0(\mathbf{x})$ on the grids $\{(x_j, y_k, z_l), (j, k, l) \in \mathcal{T}_{JKL}^0\}$ and approximating the integrals in (2.16) by a quadrature rule on the grids

[18,33]. Let ϕ_{jkl}^n and φ_{jkl}^n be the approximations of $\phi(x_j, y_k, z_l, t_n)$ and $\varphi(x_j, y_k, z_l, t_n)$, respectively, and denote $\rho_{jkl}^n = |\phi_{jkl}^n|^2$ and $V_{jkl} = V(x_j, y_k, z_l)$ for $(j, k, l) \in \mathcal{T}_{JKL}^0$. Choosing $\phi_{jkl}^0 = \phi_0(x_j, y_k, z_l)$ for $(j, k, l) \in \mathcal{T}_{JKL}^0$, for $n = 0, 1, \dots$, a backward Euler sine pseudo-spectral discretization in 3D (BESP-3D) for (2.6)–(2.7) reads:

$$\frac{\phi_{jkl}^+ - \phi_{jkl}^n}{\Delta t} = -\left(\sqrt{-\Delta^s + m^2} \phi^+\right)_{|jkl} - \left(V_{jkl} + \beta \varphi_{jkl}^n\right) \phi_{jkl}^+, \quad (j, k, l) \in \mathcal{T}_{JKL}, \tag{2.19}$$

$$-(\Delta^s \varphi^n)_{|jkl} = \rho_{jkl}^n, \quad \phi_{jkl}^{n+1} = \frac{\phi_{jkl}^+}{\|\phi^+\|_h}, \tag{2.20}$$

$$\phi_{0kl}^{n+1} = \phi_{j0l}^{n+1} = \phi_{j0l}^{n+1} = \phi_{jkl}^{n+1} = \phi_{jkl}^{n+1} = \phi_{jkl}^{n+1} = 0, \quad (j, k, l) \in \mathcal{T}_{JKL}^0, \tag{2.21}$$

$$\varphi_{0kl}^{n+1} = \varphi_{j0l}^{n+1} = \varphi_{j0l}^{n+1} = \varphi_{jkl}^{n+1} = \varphi_{jkl}^{n+1} = \varphi_{jkl}^{n+1} = 0, \quad (j, k, l) \in \mathcal{T}_{JKL}^0, \tag{2.22}$$

where Δ^s is the sine pseudospectral approximation [18,33] of the Laplacian Δ , defined as

$$-(\Delta^s \phi^n)_{|jkl} = \sum_{(p,q,s) \in \mathcal{T}_{JKL}} \Xi_{pqs}(\widehat{\phi^n})_{pqs} \Phi_{pqs}(x_j, y_k, z_l), \quad (j, k, l) \in \mathcal{T}_{JKL}$$

and the approximation to the operator $\sqrt{-\Delta + m^2}$ is defined as

$$\left(\sqrt{-\Delta^s + m^2} \phi^n\right)_{|jkl} = \sum_{(p,q,s) \in \mathcal{T}_{JKL}} \sqrt{\Xi_{pqs} + m^2}(\widehat{\phi^n})_{pqs} \Phi_{pqs}(x_j, y_k, z_l), \quad (j, k, l) \in \mathcal{T}_{JKL},$$

with

$$\Xi_{pqs} = (\mu_p^x)^2 + (\mu_q^y)^2 + (\mu_s^z)^2, \quad (p, q, s) \in \mathcal{T}_{JKL}, \tag{2.23}$$

$(\widehat{\phi^n})_{pqs}((p, q, s) \in \mathcal{T}_{JKL})$ the discrete sine transform coefficients defined as

$$(\widehat{\phi^n})_{pqs} = \frac{8}{JKL} \sum_{(j,k,l) \in \mathcal{T}_{JKL}} \phi_{jkl}^n \Phi_{pqs}(x_j, y_k, z_l), \quad (p, q, s) \in \mathcal{T}_{JKL} \tag{2.24}$$

and the discrete l^2 -norm $\|\cdot\|_h$ defined as

$$\|\phi^+\|_h^2 = h_x h_y h_z \sum_{(j,k,l) \in \mathcal{T}_{JKL}} |\phi_{jkl}^+|^2.$$

Similar as in [4,3,36], the linear system (2.19)–(2.22) can be iteratively solved efficiently in phase space with the help of discrete sine transform and we omit the details here for brevity. In fact, the above numerical method is spectrally accurate, works for general potential $V(\mathbf{x})$ and its memory cost is $O(JKL)$.

3. Numerical method for computing dynamics in 3D

In this section, we present an efficient and accurate numerical method for computing the dynamics of the RSP system (1.7)–(1.8) with the initial condition (1.2). Again, the whole space problem is truncated into a bounded computation domain $\Omega = [a, b] \times [c, d] \times [e, f]$ with homogeneous Dirichlet boundary conditions on $\partial\Omega$, i.e.

$$i\partial_t \psi = \sqrt{-\Delta + m^2} \psi + V(\mathbf{x})\psi + \beta \varphi \psi, \quad \mathbf{x} \in \Omega, \quad t > 0, \tag{3.1}$$

$$-\Delta \varphi = |\psi|^2, \quad \mathbf{x} \in \Omega, \quad \psi(\mathbf{x}, t)|_{\partial\Omega} = \varphi(\mathbf{x}, t)|_{\partial\Omega} = 0, \quad t \geq 0, \tag{3.2}$$

$$\psi(\mathbf{x}, 0) = \psi_0(\mathbf{x}), \quad \mathbf{x} \in \Omega. \tag{3.3}$$

In order to discretize the above system, we apply the time-splitting technique to decouple the nonlinearity, which was widely and successfully used for nonlinear partial differential equations [34,6,7,11,9,30,8,35,25,31,36]. From time $t = t_n$ to $t = t_{n+1}$, one first solves

$$i\partial_t \psi(\mathbf{x}, t) = \sqrt{-\Delta + m^2} \psi(\mathbf{x}, t), \quad \mathbf{x} \in \Omega, \quad \psi(\mathbf{x}, t)|_{\partial\Omega} = 0, \quad t_n \leq t \leq t_{n+1} \tag{3.4}$$

for the time step of length Δt , followed by solving

$$i\partial_t \psi(\mathbf{x}, t) = [V(\mathbf{x}) + \beta \varphi(\mathbf{x}, t)] \psi(\mathbf{x}, t), \quad \mathbf{x} \in \Omega, \quad t_n \leq t \leq t_{n+1}, \tag{3.5}$$

$$-\Delta \varphi(\mathbf{x}, t) = |\psi(\mathbf{x}, t)|^2, \quad \mathbf{x} \in \Omega, \quad \psi(\mathbf{x}, t)|_{\partial\Omega} = \varphi(\mathbf{x}, t)|_{\partial\Omega} = 0, \quad t_n \leq t \leq t_{n+1}, \tag{3.6}$$

for the same time step. Similar as (2.17), Eq. (3.4) will be discretized in space by sine spectral method [22,24,33,36], and then in phase space integrated exactly in time. For $t_n \leq t \leq t_{n+1}$, (3.5)–(3.6) leaves $|\psi|$ (and φ) invariant in time t , i.e.

$$|\psi(\mathbf{x}, t)| \equiv |\psi(\mathbf{x}, t_n)|, \quad \varphi(\mathbf{x}, t) \equiv \varphi(\mathbf{x}, t_n), \quad t_n \leq t \leq t_{n+1}, \quad \mathbf{x} \in \Omega.$$

Plugging them into (3.5) and (3.6), we obtain

$$i\partial_t \psi(\mathbf{x}, t) = [V(\mathbf{x}) + \beta\varphi(\mathbf{x}, t_n)]\psi(\mathbf{x}, t), \quad \mathbf{x} \in \Omega, \quad t_n \leq t \leq t_{n+1}, \tag{3.7}$$

$$-\Delta\varphi(\mathbf{x}, t_n) = |\psi(\mathbf{x}, t_n)|^2, \quad \mathbf{x} \in \Omega, \quad \psi(\mathbf{x}, t_n)|_{\partial\Omega} = \varphi(\mathbf{x}, t_n)|_{\partial\Omega} = 0. \tag{3.8}$$

Again, (3.8) will be discretized in space by sine spectral method and the linear ODE (3.7) will be integrated in time exactly.

Similar as Section 2.2, in practical computation, the above sine spectral method will be replaced by sine pseudospectral method [18,33]. Let ψ_{jkl}^n and φ_{jkl}^n be the approximations of $\psi(x_j, y_k, z_l, t_n)$ and $\varphi(x_j, y_k, z_l, t_n)$, respectively, and choose $\psi_{jkl}^0 = \psi_0(x_j, y_k, z_l)$ for $(j, k, l) \in \mathcal{T}_{JKL}^0$. For the convenience of readers, here we present a detailed second order time-splitting sine pseudospectral discretization in 3D (TSSP-3D) to (3.1)–(3.3) [6,7,34,8,36]:

$$\begin{aligned} \psi_{jkl}^{(1)} &= \sum_{(p,q,s) \in \mathcal{T}_{JKL}} \exp\left\{-\frac{i\Delta t}{2} \sqrt{\Xi_{pqs} + m^2}\right\} (\widetilde{\psi}^n)_{pqs} \Phi_{pqs}(x_j, y_k, z_l), \\ \psi_{jkl}^{(2)} &= \exp\left\{-i\Delta t (V_{jkl} + \beta\varphi_{jkl}^{(1)})\right\} \psi_{jkl}^{(1)}, \quad (j, k, l) \in \mathcal{T}_{JKL}, \end{aligned} \tag{3.9}$$

$$\psi_{jkl}^{n+1} = \sum_{(p,q,s) \in \mathcal{T}_{JKL}} \exp\left\{-\frac{i\Delta t}{2} \sqrt{\Xi_{pqs} + m^2}\right\} (\widetilde{\psi}^{(2)})_{pqs} \Phi_{pqs}(x_j, y_k, z_l), \quad n \geq 0,$$

where Ξ_{pqs} is defined in (2.23), $(\widetilde{\psi}^n)_{pqs}$ and $(\widetilde{\psi}^{(2)})_{pqs}$ are the discrete sine transform coefficients of ψ^n and $\psi^{(2)}$, respectively, which are defined similar as (2.24), and

$$\varphi_{jkl}^{(1)} = \sum_{(p,q,s) \in \mathcal{T}_{JKL}} \frac{1}{\Xi_{pqs}} (|\psi^{(1)}|^2)_{pqs} \Phi_{pqs}(x_j, y_k, z_l), \quad (j, k, l) \in \mathcal{T}_{JKL}.$$

The above method is explicit, spectrally accurate in space and second-order accurate in time. Its memory cost is $O(JKL)$ and computational cost per time step is $O(JKL \ln(JKL))$. It works for general potential $V(\mathbf{x})$ and initial data $\psi_0(\mathbf{x})$. In addition, following the analogue proof in [6,7], we have

Lemma 3.1. *The TSSP-3D method (3.9) is normalization conservation, i.e.,*

$$\|\psi^n\|_h^2 := h_x h_y h_z \sum_{(j,k,l) \in \mathcal{T}_{JKL}} |\psi_{jkl}^n|^2 \equiv h_x h_y h_z \sum_{(j,k,l) \in \mathcal{T}_{JKL}} |\psi_{jkl}^0|^2 = \|\psi^0\|_h^2, \quad n \geq 0.$$

Hence the method is unconditionally stable.

By using the Parseval's equality, we remark here that the energy and chemical potential can be approximated via the composite trapezoidal quadrature, i.e.

$$\begin{aligned} E(\psi(\mathbf{x}, t_n)) &\approx E_h(\psi^n) = E_h^{\text{kin}}(\psi^n) + E_h^{\text{exp}}(\psi^n) + E_h^{\text{inp}}(\psi^n), \\ \mu(\psi(\mathbf{x}, t_n)) &\approx \mu_h(\psi^n) = E_h^{\text{kin}}(\psi^n) + E_h^{\text{exp}}(\psi^n) + 2E_h^{\text{inp}}(\psi^n), \quad n \geq 0, \end{aligned}$$

where the kinetic energy, external potential energy and internal potential energy are defined as

$$\begin{aligned} E_h^{\text{kin}}(\psi^n) &= h_x h_y h_z \sum_{(j,k,l) \in \mathcal{T}_{JKL}} (\psi_{jkl}^n)^* (-\Delta^s + m^2)^{1/2} \psi_{jkl}^n = \frac{(b-a)(d-c)(f-e)}{8} \sum_{(p,q,s) \in \mathcal{T}_{JKL}} \sqrt{\Xi_{pqs} + m^2} |(\widetilde{\psi}^n)_{pqs}|^2, \\ E_h^{\text{exp}}(\psi^n) &= h_x h_y h_z \sum_{(j,k,l) \in \mathcal{T}_{JKL}} V_{jkl} |\psi_{jkl}^n|^2, \quad n \geq 0, \\ E_h^{\text{inp}}(\psi^n) &= \frac{\beta h_x h_y h_z}{2} \sum_{(j,k,l) \in \mathcal{T}_{JKL}} \varphi_{jkl}^n |\psi_{jkl}^n|^2 = \frac{(b-a)(d-c)(f-e)\beta}{16} \sum_{(p,q,s) \in \mathcal{T}_{JKL}} \frac{1}{\Xi_{pqs}} |(\widetilde{\psi}^n)_{pqs}|^2. \end{aligned}$$

4. Simplified numerical methods for spherically symmetric case

In this section, we assume that the potential V and initial data ψ_0 are spherically symmetric, i.e. $V(\mathbf{x}) = V(r)$ and $\psi_0(\mathbf{x}) = \psi_0(r)$ with $r = |\mathbf{x}|$ for $\mathbf{x} \in \mathbb{R}^3$. By using a proper change of variables, we simplify BESP-3D and TSSP-3D methods in previous sections such that the memory cost (with $J = K = L$) is reduced from $O(J^3)$ to $O(J)$ and computational cost per step is reduced from $O(J^3 \ln(J^3))$ to $O(J \ln(J))$.

4.1. Quasi-1D problems

Under the spherically symmetric assumption, the solution ψ of (1.7)–(1.8) with the initial condition (1.2) and the ground state ϕ_g are also spherically symmetric, i.e.

$$\psi(\mathbf{x}, t) = \psi(r, t), \quad \phi_g(\mathbf{x}) = \phi_g(r), \quad \mathbf{x} \in \mathbb{R}^3, \quad t \geq 0.$$

Thus, the RSP system (1.7)–(1.8) collapses to

$$i\partial_t \psi = \left[-\frac{1}{r^2} \frac{\partial}{\partial r} \left(r^2 \frac{\partial}{\partial r} \right) + m^2 \right]^{1/2} \psi + V(r)\psi + \beta\phi\psi, \quad 0 < r < \infty, \quad t > 0, \quad (4.1)$$

$$-\frac{1}{r^2} \frac{\partial}{\partial r} \left(r^2 \frac{\partial \phi}{\partial r} \right) = |\psi|^2, \quad 0 < r < \infty, \quad \lim_{r \rightarrow \infty} \phi(r, t) = 0, \quad t \geq 0, \quad (4.2)$$

$$\partial_r \psi(0, t) = \partial_r \phi(0, t) = 0, \quad t \geq 0, \quad (4.3)$$

with initial condition

$$\psi(r, 0) = \psi_0(r), \quad 0 \leq r < \infty. \quad (4.4)$$

Also, the normalization (1.4) collapses to

$$N(\psi(\cdot, t)) = 4\pi \int_0^\infty |\psi(r, t)|^2 r^2 dr \equiv 4\pi \int_0^\infty |\psi_0(r)|^2 r^2 dr = 1, \quad t \geq 0 \quad (4.5)$$

and the energy (1.9) collapses to

$$E(\psi(\cdot, t)) = 4\pi \int_0^\infty \left[\psi^* \left(-\frac{1}{r^2} \frac{\partial}{\partial r} \left(r^2 \frac{\partial}{\partial r} \right) + m^2 \right)^{1/2} \psi + \left(V(r) + \frac{\beta}{2} \phi \right) |\psi|^2 \right] r^2 dr \equiv E(\psi_0), \quad t \geq 0.$$

Introducing

$$\bar{\psi}(r, t) = 2\sqrt{\pi r} \psi(r, t), \quad \bar{\phi}(r, t) = 4\pi r \phi(r, t), \quad 0 \leq r < \infty, \quad t \geq 0, \quad (4.6)$$

a detailed computation leads to

$$\left[-\frac{1}{r^2} \frac{\partial}{\partial r} \left(r^2 \frac{\partial}{\partial r} \right) + m^2 \right]^{1/2} \bar{\psi} = \frac{1}{2\sqrt{\pi r}} (-\partial_{rr} + m^2)^{1/2} \bar{\psi},$$

$$\frac{1}{r^2} \frac{\partial}{\partial r} \left(r^2 \frac{\partial \phi}{\partial r} \right) = \frac{1}{4\pi r} \partial_{rr} \bar{\phi}, \quad 0 < r < \infty, \quad t > 0.$$

Plugging the above equations and (4.6) into (4.1)–(4.3), we obtain

$$i\partial_t \bar{\psi} = (-\partial_{rr} + m^2)^{1/2} \bar{\psi} + V(r)\bar{\psi} + \frac{\beta}{4\pi r} \bar{\phi} \bar{\psi}, \quad 0 < r < \infty, \quad t > 0, \quad (4.7)$$

$$-\partial_{rr} \bar{\phi} = \frac{1}{r} |\bar{\psi}|^2, \quad 0 < r < \infty, \quad \lim_{r \rightarrow \infty} \bar{\phi}(r, t) = 0, \quad t \geq 0, \quad (4.8)$$

$$\bar{\psi}(0, t) = \bar{\phi}(0, t) = 0, \quad t \geq 0, \quad (4.9)$$

with initial condition

$$\bar{\psi}(r, 0) = \bar{\psi}_0(r) = 2\sqrt{\pi r} \psi_0(r), \quad 0 \leq r < \infty. \quad (4.10)$$

Again, it is easy to show that the above problem conserves the mass

$$\bar{N}(\bar{\psi}(\cdot, t)) := \|\bar{\psi}(\cdot, t)\|^2 = \int_0^\infty |\bar{\psi}(r, t)|^2 dr \equiv \int_0^\infty |\bar{\psi}_0(r)|^2 dr, \quad t \geq 0, \quad (4.11)$$

and the energy

$$\bar{E}(\bar{\psi}(\cdot, t)) := \int_0^\infty \left[\bar{\psi}^* (-\partial_{rr} + m^2)^{1/2} \bar{\psi} + \left(V(r) + \frac{\beta}{8\pi r} \bar{\phi} \right) |\bar{\psi}|^2 \right] dr \equiv \bar{E}(\bar{\psi}_0), \quad t \geq 0. \quad (4.12)$$

Plugging (4.6) into (4.11) and (4.12), we get

$$N(\psi(\cdot, t)) = \bar{N}(\bar{\psi}(\cdot, t)) \equiv 1, \quad E(\psi(\cdot, t)) = \bar{E}(\bar{\psi}(\cdot, t)), \quad t \geq 0.$$

After we get the solution $\bar{\psi}$ of (4.7)–(4.10), the solution ψ of (4.1)–(4.4) can be obtained as

$$\psi(r, t) = \frac{1}{2\sqrt{\pi}} \begin{cases} \bar{\psi}(r, t)/r, & r > 0, \\ \partial_r \bar{\psi}(0, t) = \lim_{s \rightarrow 0^+} \bar{\psi}(s, t)/s, & r = 0, \end{cases} \quad t \geq 0.$$

Meanwhile, the minimization problem (1.6) for ground state collapses to:

Find $\bar{\phi}_g \in \bar{S} = \{\bar{\phi} | \bar{\phi} \in H^{1/2}([0, \infty)), \bar{\phi}(0) = 0, \|\bar{\phi}\|^2 = \int_0^\infty |\bar{\phi}|^2 dr = 1\}$ such that

$$\bar{E}_g := \bar{E}(\bar{\phi}_g) = \min_{\bar{\phi} \in \bar{S}} \bar{E}(\bar{\phi}). \tag{4.13}$$

Again, after we get the ground state $\bar{\phi}_g$ of (4.13), the solution ϕ_g of (1.6) can be obtained as

$$\phi_g(r) = \frac{1}{2\sqrt{\pi}} \begin{cases} \bar{\phi}_g(r)/r, & r > 0, \\ \partial_r \bar{\phi}_g(0) = \lim_{s \rightarrow 0^+} \bar{\phi}_g(s)/s, & r = 0. \end{cases}$$

4.2. Sine pseudospectral discretization in 1D

Similar as Section 2, for computing the minimizer of (4.13), we construct the following gradient flow with discrete normalization in 1D (GFDN-1D):

$$\partial_t \bar{\phi} = -(-\partial_{rr} + m^2)^{1/2} \bar{\phi} - V(r) \bar{\phi} - \frac{\beta}{4\pi r} \bar{\phi} \bar{\phi}, \quad 0 < r < \infty, \quad t_n \leq t < t_{n+1}, \tag{4.14}$$

$$-\partial_{rr} \bar{\phi} = \frac{1}{r} |\bar{\phi}|^2, \quad 0 < r < \infty, \quad \lim_{r \rightarrow \infty} \bar{\phi}(r, t) = 0, \quad t \geq 0, \tag{4.15}$$

$$\bar{\phi}(r, t_{n+1}) := \bar{\phi}(r, t_{n+1}^+) = \frac{\bar{\phi}(r, t_{n+1}^-)}{\|\bar{\phi}(r, t_{n+1}^-)\|}, \quad n \geq 0, \tag{4.16}$$

$$\bar{\phi}(0, t) = \bar{\phi}(0, t) = 0, \quad t \geq 0, \tag{4.17}$$

$$\bar{\phi}(r, 0) = \bar{\phi}_0(r), \quad 0 \leq r < \infty, \quad \text{with} \quad \|\bar{\phi}_0\|^2 = \int_0^\infty |\bar{\phi}_0(r)|^2 dr = 1, \tag{4.18}$$

where $\bar{\phi}(r, t_n^\pm) := \lim_{t \rightarrow t_n^\pm} \bar{\phi}(r, t)$ for $0 \leq r < \infty$.

Again, in practical computation, the above GFDN-1D will be truncated into an interval $[0, R]$ with $R > 0$ sufficiently large with homogeneous Dirichlet boundary conditions

$$\bar{\phi}(R, t) = \bar{\phi}(R, t) = 0, \quad t \geq 0.$$

Then it is discretized in space by sine pseudospectral method and in time by back Euler method. Let $J > 0$ be an even integer, choose mesh size $h_r = R/J$, and denote grid points as $r_j = jh_r$ for $j = 0, 1, \dots, J$. Let $\bar{\phi}_j^n$ and $\bar{\varphi}_j^n$ be the approximations of $\bar{\phi}(r_j, t_n)$ and $\bar{\varphi}(r_j, t_n)$, respectively, denote $V_j = V(r_j)$ for $j = 0, 1, \dots, J$ and $\rho_j^n = |\bar{\phi}_j^n|^2 / r_j$ for $j = 1, 2, \dots, J-1$. Choosing $\bar{\phi}_j^0 = \bar{\phi}_0(r_j)$ for $j = 0, 1, \dots, J$, for $n = 0, 1, \dots$, a backward Euler sine pseudospectral discretization in 1D (BESP-1D) reads:

$$\frac{\bar{\phi}_j^{n+1} - \bar{\phi}_j^n}{\Delta t} = -\left(\sqrt{-\partial_{rr}^s + m^2} \bar{\phi}^n\right)\Big|_j - \left(V_j + \frac{\beta}{4\pi r_j} \bar{\varphi}_j^n\right) \bar{\phi}_j^{n+1}, \quad j = 1, 2, \dots, J-1, \tag{4.19}$$

$$-(\partial_{rr}^s \bar{\phi}^n)\Big|_j = \rho_j^n, \quad j = 1, 2, \dots, J-1, \quad \bar{\phi}_0^{n+1} = \bar{\phi}_0^n = \bar{\varphi}_0 = \bar{\varphi}_J = 0, \tag{4.20}$$

$$\bar{\phi}_j^{n+1} = \frac{\bar{\phi}_j^{n+1}}{\|\bar{\phi}^{n+1}\|_h}, \quad j = 0, 1, \dots, J, \quad \text{with} \quad \|\bar{\phi}^{n+1}\|_h^2 := h_r \sum_{j=1}^{J-1} |\bar{\phi}_j^{n+1}|^2, \tag{4.21}$$

where ∂_{rr}^s is the sine pseudospectral approximation of ∂_{rr} , defined as

$$-(\partial_{rr}^s \bar{\phi}^n)\Big|_j = \sum_{k=1}^{J-1} (\mu_k^r)^2 (\bar{\phi}^n)_k \sin\left(\frac{jk\pi}{J}\right), \quad j = 0, 1, \dots, J$$

and the approximation to the operator $\sqrt{-\partial_{rr} + m^2}$ is defined as

$$\left(\sqrt{-\partial_{rr}^s + m^2} \bar{\phi}^n\right)\Big|_j = \sum_{k=1}^{J-1} \sqrt{(\mu_k^r)^2 + m^2} (\bar{\phi}^n)_k \sin\left(\frac{jk\pi}{J}\right), \quad j = 0, 1, \dots, J,$$

with

$$\mu_k^r = \frac{k\pi}{R}, \quad k = 1, 2, \dots, J-1$$

and $(\bar{\phi}^n)_k (k = 1, 2, \dots, J-1)$ the discrete sine transform coefficients defined as

$$(\widetilde{\phi^n})_k = \frac{2}{J} \sum_{j=1}^{J-1} \phi_j^n \sin\left(\frac{jk\pi}{J}\right), \quad k = 1, 2, \dots, J-1. \quad (4.22)$$

Again, the linear system (4.19)–(4.21) can be iteratively solved efficiently in phase space with the help of discrete sine transform [4,36]. The above numerical method is spectrally accurate and it works only when $V(\mathbf{x})$ is spherically symmetric, and its memory cost is only $O(J)$.

Similar as Section 3, for computing the dynamics of (4.7)–(4.10), we first apply the time-splitting technique to decouple the nonlinearity and then use sine pseudospectral method to discretize the spatial derivative. Let $\bar{\psi}_j^n$ and $\bar{\varphi}_j^n$ be the approximations of $\bar{\psi}(r_j, t_n)$ and $\bar{\varphi}(r_j, t_n)$, respectively, and choose $\bar{\psi}_j^0 = \bar{\psi}_0(r_j)$ for $j = 0, 1, \dots, J$. Then a second-order time-splitting sine pseudospectral discretization in 1D (TSSP-1D) [6,7,34,36] to (4.7)–(4.10) reads

$$\begin{aligned} \bar{\psi}_j^{(1)} &= \sum_{k=1}^{J-1} \exp\left\{-\frac{i\Delta t}{2} \sqrt{(\mu_k^r)^2 + m^2}\right\} (\widetilde{\bar{\psi}^n})_k \sin\left(\frac{jk\pi}{J}\right), \\ \bar{\psi}_j^{(2)} &= \exp\left\{-i\Delta t \left(V_j + \frac{\beta}{4\pi r_j} \bar{\varphi}^{(1)}\right)\right\} \bar{\psi}_j^{(1)}, \quad j = 1, 2, \dots, J-1, \\ \bar{\psi}_j^{n+1} &= \sum_{k=1}^{J-1} \exp\left\{-\frac{i\Delta t}{2} \sqrt{(\mu_k^r)^2 + m^2}\right\} (\widetilde{\bar{\psi}^{(2)}})_k \sin\left(\frac{jk\pi}{J}\right), \quad n \geq 0, \end{aligned} \quad (4.23)$$

where $(\widetilde{\bar{\psi}^n})_k$ and $(\widetilde{\bar{\psi}^{(2)}})_k$ are the discrete sine transform coefficients of $\bar{\psi}^n$ and $\bar{\psi}^{(2)}$, respectively, which are defined similar as (4.22), and

$$\bar{\varphi}_j^{(1)} = \sum_{k=1}^{J-1} \frac{1}{(\mu_k^r)^2} (\widetilde{\rho^n})_k \sin\left(\frac{jk\pi}{J}\right), \quad j = 1, 2, \dots, J-1,$$

with $\rho_j^n = |\bar{\psi}^{(1)}|^2 / r_j$ for $j = 1, 2, \dots, J-1$.

Again, the above method is explicit, spectrally accurate in space and second-order accurate in time, its memory cost is $O(J)$ and computational cost per time step is $O(\ln(J))$. It works only when the potential $V(\mathbf{x})$ and initial data $\psi_0(\mathbf{x})$ are spherically symmetric. In addition, following the analogue proof in [6,7], we have.

Lemma 4.1. *The TSSP-1D method (4.23) is normalization conservation, i.e.,*

$$\|\bar{\psi}^n\|_h^2 := h_r \sum_{j=1}^{J-1} |\bar{\psi}_j^n|^2 \equiv h_r \sum_{j=1}^{J-1} |\bar{\psi}_j^0|^2 = \|\bar{\psi}^0\|_h^2, \quad n \geq 0.$$

After we get the solution $\bar{\psi}_j^n$ from (4.23), the solution ψ_j^n of (4.1)–(4.4) can be obtained as

$$\psi_j^n = \frac{1}{2\sqrt{\pi}} \begin{cases} \bar{\psi}_j^n / r_j, & j = 1, 2, \dots, J, \\ \sum_{k=1}^{J-1} \mu_k^r (\widetilde{\bar{\psi}^n})_k, & j = 0, \end{cases} \quad n \geq 0.$$

And after we get the ground state $(\bar{\phi}_g)_j (j = 0, 1, \dots, J)$ from (4.19)–(4.21), the solution $(\phi_g)_j (j = 0, 1, \dots, J)$ of (1.6) can be obtained as

$$(\phi_g)_j = \frac{1}{2\sqrt{\pi}} \begin{cases} (\bar{\phi}_g)_j / r_j, & j = 1, 2, \dots, J, \\ \sum_{k=1}^{J-1} \mu_k^r (\widetilde{\bar{\phi}_g})_k, & j = 0, \end{cases}$$

where $(\widetilde{\bar{\psi}^n})_k$ and $(\widetilde{\bar{\phi}_g})_k$ are the discrete sine transform coefficients of $\bar{\psi}^n$ and $\bar{\phi}_g$, respectively.

By using the Parseval equality, we remark here that the energy and chemical potential can also be approximated via the composite trapezoidal quadrature, i.e.

$$\begin{aligned} E(\psi(\mathbf{x}, t_n)) &\approx \bar{E}_h(\bar{\psi}^n) = \bar{E}_h^{\text{kin}}(\bar{\psi}^n) + \bar{E}_h^{\text{exp}}(\bar{\psi}^n) + \bar{E}_h^{\text{inp}}(\bar{\psi}^n), \\ \mu(\psi(\mathbf{x}, t_n)) &\approx \bar{\mu}_h(\bar{\psi}^n) = \bar{E}_h^{\text{kin}}(\bar{\psi}^n) + \bar{E}_h^{\text{exp}}(\bar{\psi}^n) + 2\bar{E}_h^{\text{inp}}(\bar{\psi}^n), \quad n \geq 0, \end{aligned}$$

where the kinetic energy, external potential energy and internal potential energy are defined as

$$\bar{E}_h^{\text{kin}}(\bar{\psi}^n) = h_r \sum_{j=1}^{J-1} \left(\bar{\psi}_j^n \right) * \left(-\partial_{rr}^s + m^2 \right)^{1/2} \bar{\psi}_j^n = \frac{R}{2} \sum_{k=1}^{J-1} \sqrt{(\mu_k^r)^2 + m^2} \left| \left(\bar{\psi}^n \right)_k \right|^2,$$

$$\bar{E}_h^{\text{exp}}(\bar{\psi}^n) = h_r \sum_{j=1}^{J-1} V_j \left| \bar{\psi}_{jkl}^n \right|^2, \quad n \geq 0,$$

$$\bar{E}_h^{\text{inp}}(\bar{\psi}^n) = \frac{\beta h_r}{8\pi} \sum_{j=1}^{J-1} \bar{\varphi}_j^n \left(\frac{1}{r_j} \left| \bar{\psi}_j^n \right|^2 \right) = \frac{\beta R}{16\pi} \sum_{k=1}^{J-1} \frac{1}{(\mu_k^r)^2} \left| \left(\bar{\rho}^n \right)_k \right|^2,$$

with $\rho_j^n = \left| \bar{\psi}_j^n \right|^2 / r_j$ for $j = 1, 2, \dots, J - 1$.

4.3. Finite difference discretization in 1D

For comparison, a backward Euler finite difference (BEFD-1D) discretization can be applied to (4.14)–(4.18) after it is truncated on the interval $[0, R]$ as

$$\frac{\bar{\phi}^+ - \bar{\phi}^n}{\Delta t} = -(A + m^2 I_{J-1})^{1/2} \bar{\phi}^+ - F^n \bar{\phi}^+, \quad n \geq 0, \tag{4.24}$$

$$A \varphi^n = \rho^n, \quad \bar{\phi}^{n+1} = \frac{\bar{\phi}^+}{\| \bar{\phi}^+ \|_h}, \quad n \geq 0, \quad \bar{\phi}^0 = \bar{\phi}_0, \tag{4.25}$$

where I_{J-1} is the $(J - 1) \times (J - 1)$ identity matrix, $\bar{\phi}^+ = (\bar{\phi}_1^+, \bar{\phi}_2^+, \dots, \bar{\phi}_{J-1}^+)^T$, $\bar{\phi}^n = (\bar{\phi}_1^n, \bar{\phi}_2^n, \dots, \bar{\phi}_{J-1}^n)^T$, $\bar{\varphi}^n = (\bar{\varphi}_1^n, \bar{\varphi}_2^n, \dots, \bar{\varphi}_{J-1}^n)^T$, $\bar{\phi}_0 = (\bar{\phi}_0(r_1), \bar{\phi}_0(r_2), \dots, \bar{\phi}_0(r_{J-1}))^T$, $\rho^n = (|\bar{\phi}_1^n|^2 / r_1, |\bar{\phi}_2^n|^2 / r_2, \dots, |\bar{\phi}_{J-1}^n|^2 / r_{J-1})^T$, $F^n = \text{diag}\{V_1 + \beta \bar{\varphi}_1^n / 4\pi r_1, \dots, V_{J-1} + \beta \bar{\varphi}_{J-1}^n / 4\pi r_{J-1}\}$, and A is a $(J - 1) \times (J - 1)$ tri-diagonal matrix defined as

$$A = \frac{1}{h_r^2} \begin{pmatrix} 2 & -1 & 0 & \dots & 0 \\ -1 & 2 & -1 & \dots & 0 \\ 0 & -1 & 2 & \dots & 0 \\ \vdots & \vdots & \vdots & \ddots & \vdots \\ 0 & 0 & 0 & -1 & 2 \end{pmatrix}.$$

In computation, we need factorized A as $A = Q \mathcal{A} Q^T$ with \mathcal{A} a diagonal matrix and Q an orthogonal matrix satisfying $Q^T = Q^{-1}$, then $(A + m^2 I_{J-1})^{1/2} = Q(\mathcal{A} + m^2 I_{J-1})^{1/2} Q^T$.

Similarly, we can apply a time-splitting finite difference (TSFD-1D) discretization to (4.7)–(4.10) for dynamics after it is truncated on the interval $[0, R]$. We omit the details here for brevity.

Remark 4.1. If the Poisson Eq. (1.8) in the RSP system is replaced by the Yukawa equation

$$-\Delta \varphi + \beta \varphi = |\psi|^2, \quad \mathbf{x} \in \mathbb{R}^3, \quad \lim_{|\mathbf{x}| \rightarrow \infty} \varphi(\mathbf{x}, t) = 0, \quad t \geq 0,$$

with $\beta > 0$ a constant, our numerical methods BEFD-3D and BEFD-1D for computing ground states and TSSP-3D and TSSP-1D for computing dynamics can be extended straightforward.

Remark 4.2. For the semirelativistic Hartree system considered in [2], i.e.

$$i \varepsilon \partial_t \psi_j^\varepsilon(\mathbf{x}, t) = \left[\sqrt{-\varepsilon^2 \Delta + 1} + V^\varepsilon(\mathbf{x}) + \varphi^\varepsilon \right] \psi_j^\varepsilon, \quad \mathbf{x} \in \mathbb{R}^3, \quad t > 0, \quad |j| \leq M, \tag{4.26}$$

$$-\Delta \varphi^\varepsilon = \rho^\varepsilon := \sum_{j=-M}^M |\psi_j^\varepsilon|^2, \quad \mathbf{x} \in \mathbb{R}^3, \quad \lim_{|\mathbf{x}| \rightarrow \infty} \varphi^\varepsilon(\mathbf{x}, t) = 0, \quad t \geq 0; \tag{4.27}$$

with $\varepsilon > 0$ a scaled Planck constant and $M \geq 0$ a non-negative integer, our numerical methods TSSP-3D and TSSP-1D for computing dynamics can be extended straightforward.

5. Numerical results

In this section, we first test the accuracy of methods BEFD-3D, BEFD-1D and BEFD-1D for computing the ground state, and TSSP-3D, TSSP-1D and TSFD-1D for computing the dynamics of the RSP system. Then we apply them to simulate the ground state and dynamics in different parameter regimes and external potential, as well as with finite time blow-up. For simplification, we always choose $h_x = h_y = h_z := h$ in 3D in our computation.

5.1. Accuracy test

First, we test the spatial discretization errors of BESP-3D, BESP-1D and BEFD-1D methods for computing the ground state. In order to do so, we take $\beta = -16$, $m = 1$, $V(\mathbf{x}) \equiv 0$ for $\mathbf{x} \in \mathbb{R}^3$ in (1.7). In our computation, we choose $\Delta t = 0.01$, initial data $\phi_0(\mathbf{x}) = \frac{1}{(\pi/2)^{3/4}} e^{-(x^2+y^2+z^2)}$ in (2.9), $\Omega = [-16, 16]^3$ with $J = K = L$ (or $h_x = h_y = h_z = h$) for the 3D case; and respectively, $\bar{\phi}_0(r) = \frac{2\sqrt{\pi r}}{(\pi/2)^{3/4}} e^{-r^2}$ in (4.18), $R = 16$ for the 1D case. The ground state ϕ_g is reached when $\|\phi^n - \phi^{n+1}\|_\infty < 10^{-9}$. The “exact” ground state ϕ_g^e is obtained under a very fine mesh. Let ϕ_g^h be the numerical ground state under the mesh size h . Table 1 lists the errors $\|\phi_g^h - \phi_g^e\|_\infty$ by using BESP-3D, BESP-1D and BEFD-1D with different mesh sizes h .

Then we test the spatial and temporal discretization errors of TSSP-3D, TSSP-1D and TSFD-1D methods for computing the dynamics. Again, we take $\beta = -16$, $m = 1$, $V(\mathbf{x}) \equiv 0$ for $\mathbf{x} \in \mathbb{R}^3$ in (1.7), and the initial data $\psi_0(\mathbf{x}) = \frac{1}{(\pi/2)^{3/4}} e^{-(x^2+y^2+z^2)}$ in (1.2) and $\bar{\psi}_0(r) = \frac{2\sqrt{\pi r}}{(\pi/2)^{3/4}} e^{-r^2}$ in (4.10). In our computation, we take $\Omega = [-6, 6]^3$ with $J = K = L$ (or $h_x = h_y = h_z = h$) for the 3D case; and respectively, $R = 6$ for the 1D case. The “exact” solution ψ^e is obtained under a very fine mesh and small time step. Let $\psi^{h,\Delta t}$ be the numerical solution under the mesh size h and time step Δt . Table 2 gives the errors $\|\psi^{h,\Delta t} - \psi^e\|_\infty$ at time $t = 1$ under $\Delta t = 10^{-5}$ by using TSSP-3D, TSSP-1D and TSFD-1D with different mesh sizes h , which demonstrates spatial discretization errors; and Table 3 shows similar results under $h = 1/8$ for TSSP-3D, TSSP-1D, and respectively, $h = 1/512$ for TSFD-1D with different time steps Δt , which demonstrates temporal discretization errors.

From Tables 1–3, we can draw the following conclusions: (i). both BESP-3D and BESP-1D are spectrally accurate and BEFD-1D is second-order accurate in spatial discretization for computing the ground state; (ii). both TSSP-3D and TSSP-1D are spectrally accurate and TSFD-1D is second-order accurate in spatial discretization for computing the dynamics, and all these three methods are second-order accurate in temporal discretization. Based on these observations, for computing ground states of the RSP system, if the potential V is spherically symmetric, we suggest to use BESP-1D, otherwise, BESP-3D should be used; and for computing the dynamics, if the potential V and initial data ψ_0 are both spherically symmetric, we suggest to use TSSP-1D, otherwise, TSSP-3D should be used.

5.2. Ground states of the RSP system

To quantify the ground state $\phi_g(\mathbf{x})$, we will use its total energy $E_g := E(\phi_g)$, chemical potential $\mu_g := \mu(\phi_g)$, kinetic energy $E_g^{\text{kin}} := E^{\text{kin}}(\phi_g)$, external potential energy $E_g^{\text{exp}} := E^{\text{exp}}(\phi_g)$ and internal potential energy $E_g^{\text{inp}} := E^{\text{inp}}(\phi_g)$ as well as its mean width square δ_r defined as

$$\delta_r = \frac{1}{3} \int_{\mathbb{R}^3} |\mathbf{x}|^2 |\phi_g(\mathbf{x})|^2 \, d\mathbf{x} = \frac{1}{3} \int_{\mathbb{R}^3} (x^2 + y^2 + z^2) |\phi_g(\mathbf{x})|^2 \, d\mathbf{x},$$

Table 1
Spatial discretization error analysis of BESP-3D, BESP-1D and BEFD-1D for computing ground state.

	$h = 2$	$h = 4/3$	$h = 1$	$h = 2/3$	$h = 1/2$
BESP-3D	1.3254E-2	9.3079E-5	1.2608E-6	1.4965E-9	<E-9
BESP-1D	3.2523E-2	3.4154E-4	8.9687E-6	5.7715E-9	<E-9
	$h = 1/2$	$h = 1/4$	$h = 1/8$	$h = 1/16$	$h = 1/32$
BEFD-1D	1.0394E-2	2.4597E-3	6.0795E-4	1.5157E-4	3.7867E-5

Table 2
Spatial discretization error analysis of TSSP-3D, TSSP-1D and TSFD-1D for computing dynamics.

	$h = 1$	$h = 2/3$	$h = 1/2$	$h = 1/3$	$h = 1/4$
TSSP-3D	2.7987E-2	6.6190E-3	4.0541E-6	6.7901E-7	7.6630E-9
TSSP-1D	8.9639E-3	5.9967E-4	6.5654E-5	1.0935E-7	6.8056E-10
	$h = 1/4$	$h = 1/8$	$h = 1/16$	$h = 1/32$	$h = 1/64$
TSFD-1D	1.1365E-2	3.3655E-3	8.7813E-4	2.2189E-4	5.5622E-5

Table 3
Temporal discretization error analysis of TSSP-3D, TSSP-1D and TSFD-1D for computing dynamics.

	$k = 0.2$	$k = 0.1$	$k = 0.05$	$k = 0.025$
TSSP-3D	2.3918E-4	5.9753E-5	1.4892E-5	3.7201E-6
TSSP-1D	1.7504E-4	4.3414E-5	1.0832E-5	2.5067E-6
TSFD-1D	1.8826E-4	4.6948E-5	1.1975E-5	3.2543E-6

which can be computed numerically in 3D as

$$\delta_r \approx \frac{h_x h_y h_z}{3} \sum_{(j,k,l) \in \mathcal{T}_{JKL}} (x_j^2 + y_k^2 + z_l^2) |(\phi_g)_{jkl}|^2,$$

and respectively, if ϕ_g is spherically symmetric in 1D as

$$\delta_r \approx \frac{4\pi h_r}{3} \sum_{j=1}^{J-1} r_j^4 |(\phi_g)_j|^2.$$

Example 1. Ground states of the RSP system with spherically symmetric potential for different parameters m and β , i.e. we consider three cases: (i). $\beta = -10$ and $V(\mathbf{x}) \equiv 0$ with different m ; (ii). $m = 1$ and $V(\mathbf{x}) \equiv 0$ with different $\beta < 0$; and (iii). $m = 1$ and a harmonic trapping potential $V = \frac{1}{2}(x^2 + y^2 + z^2) = \frac{1}{2}r^2$ with different $\beta \geq 0$. The problem is always computed on a sufficiently large bounded domain $\Omega = [0, R]$ by using BESP-1D with 257 grid points and time step $\Delta t = 0.01$. The initial data $\bar{\phi}_0$ is taken as $\bar{\phi}_0 = \frac{2\sqrt{\pi}r}{(\pi/2)^{3/4}} e^{-r^2}$.

Tables 4–6 show various quantities of the ground state in cases (i), (ii) and (iii), respectively, including total energy, kinetic energy, internal and external potential energy, chemical potential μ_g and mean width square δ_r . Fig. 1 depicts the plots of the ground state solution $\phi_g(r)$ in cases (i), (ii) and (iii) as well as the energy evolution while solving the gradient flow in case (i). In addition, from the results in cases (i) and (ii), we can numerically predict the “Chandrasekhar limit mass”, λ_{cr} . For each fixed $m > 0$, we can numerically fit a curve of δ_r versus $\beta < 0$, and then λ_{cr} is numerically obtained by finding the zero point of the fitting function. Fig. 2 shows the fitting curves of δ_r versus $\beta < 0$ when $m = 2, 3$ and 4; and the ground states $\phi_g(r)$ when $m = 4$ for $\beta = -32, -32.5, -33, -33.5$. From our numerical results, it is numerically found that $\beta_{cr} = -4\pi \lambda_{cr} \approx -33.8$, i.e., $\lambda_{cr} \approx 2.69$, which is independent of m .

Table 4
Various quantities of the ground state when $\beta = -10$ and $V(\mathbf{x}) \equiv 0$ with different m for case (i) in Example 1.

m	E_g	E_g^{kin}	E_g^{inp}	μ_g	δ_r
1	0.9769	1.0380	-0.0611	0.9157	9.9553
2	1.9413	2.0761	-0.1347	1.8066	2.4889
3	2.9265	3.1141	-0.1876	2.7389	1.1062
4	3.9075	4.1521	-0.2446	3.6630	0.6222
5	4.8886	5.1902	-0.3016	4.5870	0.3982
6	5.8663	6.2282	-0.3619	5.5044	0.2765

Table 5
Various quantities of the ground state when $m = 1$ and $V(\mathbf{x}) \equiv 0$ with different $\beta < 0$ for case (ii) in Example 1.

β	E_g	E_g^{kin}	E_g^{inp}	μ_g	δ_r
-16	0.9434	1.1153	-0.1718	0.7716	3.1277
-14	0.9588	1.0825	-0.1237	0.8351	4.4562
-12	0.9679	1.0573	-0.0894	0.8785	6.5188
-10	0.9769	1.0380	-0.0611	0.9157	9.9553
-8	0.9842	1.0235	-0.0393	0.9449	16.3002
-6	0.9925	1.0128	-0.0204	0.9721	30.0289

Table 6
Various quantities of the ground state when $m = 1$ and $V(\mathbf{x}) = V(r) = \frac{1}{2}r^2$ with different $\beta > 0$ for case (iii) in Example 1.

β	E_g	E_g^{kin}	E_g^{inp}	E_g^{exp}	μ_g	δ_r
16	2.7164	1.5673	0.4408	0.7083	3.1572	0.4722
32	3.1292	1.4899	0.7764	0.8629	3.9055	0.5752
64	3.8349	1.4016	1.2947	1.1387	5.1296	0.7591
128	4.9784	1.3176	2.0488	1.6120	7.0271	1.0747
256	6.7429	1.2479	3.0960	2.3989	9.8390	1.5993
512	9.3476	1.1934	4.4745	3.6798	13.8221	2.4532

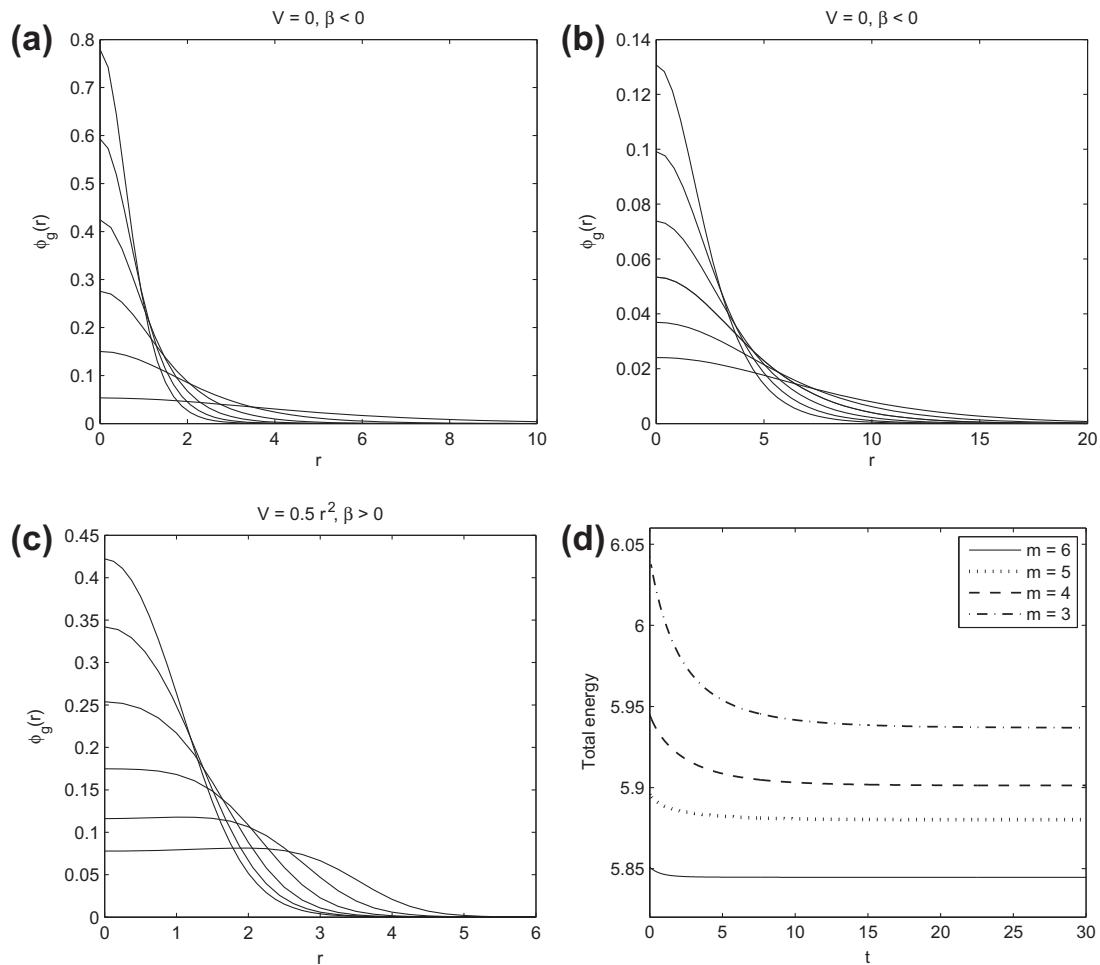


Fig. 1. Ground states $\phi_g(r)$ in Example 1: (a) for case (i) with $m = 1, 2, \dots, 6$ (as peak increasing); (b) for case (ii) with $\beta = -6, -8, \dots, -16$ (as peak increasing); (c) for case (iii) with $\beta = 2^4, 2^5, \dots, 2^9$ (as peak decreasing); and (d) time evolution of the energy in case (i) by using BESP-1D with $\bar{E}_h(\bar{\phi}^n)$ for $m = 6, \bar{E}_h(\bar{\phi}^n) + 1$ for $m = 5, \bar{E}_h(\bar{\phi}^n) + 2$ for $m = 4$ and $\bar{E}_h(\bar{\phi}^n) + 3$ for $m = 3$.

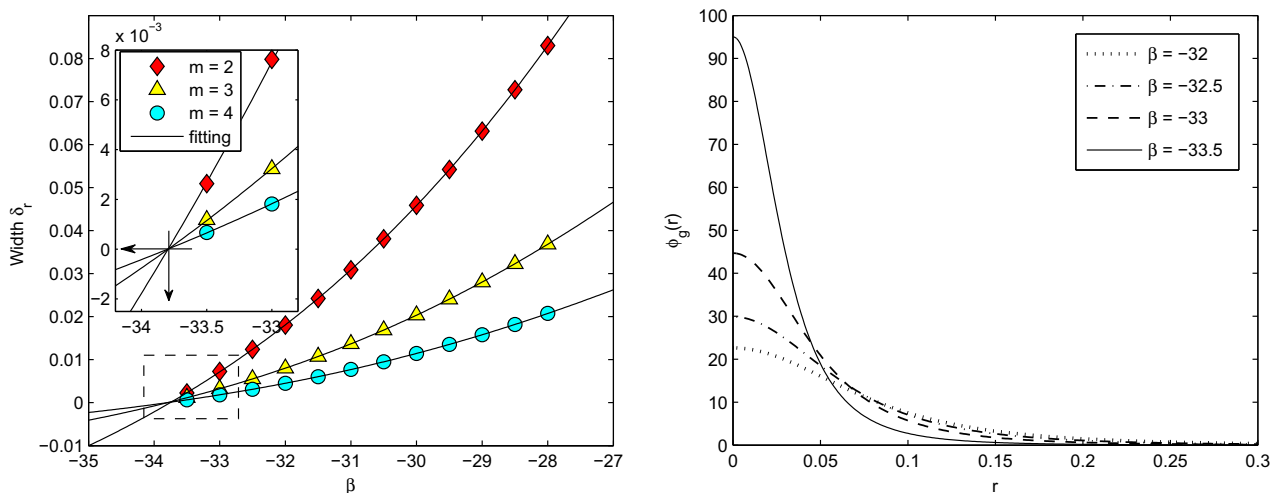


Fig. 2. Numerical study of the “Chandrasekhar limit mass”, i.e., $\lambda_{cr} = -\beta_{cr}/4\pi \approx 33.8/4\pi \approx 2.69$ in Example 1: fitting curves of δ_r versus $\beta < 0$ for $m = 2, 3$ and 4 (left column); and ground states $\phi_g(r)$ when $m = 4$ for $\beta = -32, -32.5, -33, -33.5$ (right column).

Based on Tables 4–6, and Figs. 1 and 2, we can conclude, for a large system with attractive self-interaction (i.e., $\lambda < 0$ in (1.1) or $\beta < 0$ in (1.7)) and without external potential, that: (i) as the particle mass m increases but for a fixed β in (1.7), the total energy, kinetic energy in ground state and the chemical potential increase, but the internal potential energy (negative)

decreases. Also, as m increases, the attractive interaction becomes stronger; (ii) for fixed m , as $|\beta|$ increases in (1.7), the total energy, internal potential energy (negative) in the ground state and chemical potential decrease, but the kinetic energy increases. Again, as $|\beta|$ increases, the attractive interaction becomes stronger, which also indicates that when the total mass exceeds certain critical value, the “gravitational collapse” of boson stars would occur. On the other hand, in a large system with repulsive self-interaction (i.e., $\lambda > 0$ in (1.1) or $\beta > 0$ in (1.7)) with a harmonic potential, for the fixed particle mass m as the total number of particle increase (i.e., β increases in (1.7)), the total energy, both internal and external potential energy in the ground state, and the chemical potential increase, while the kinetic energy decreases. Also, in this case the repulsive interaction becomes stronger as β increases.

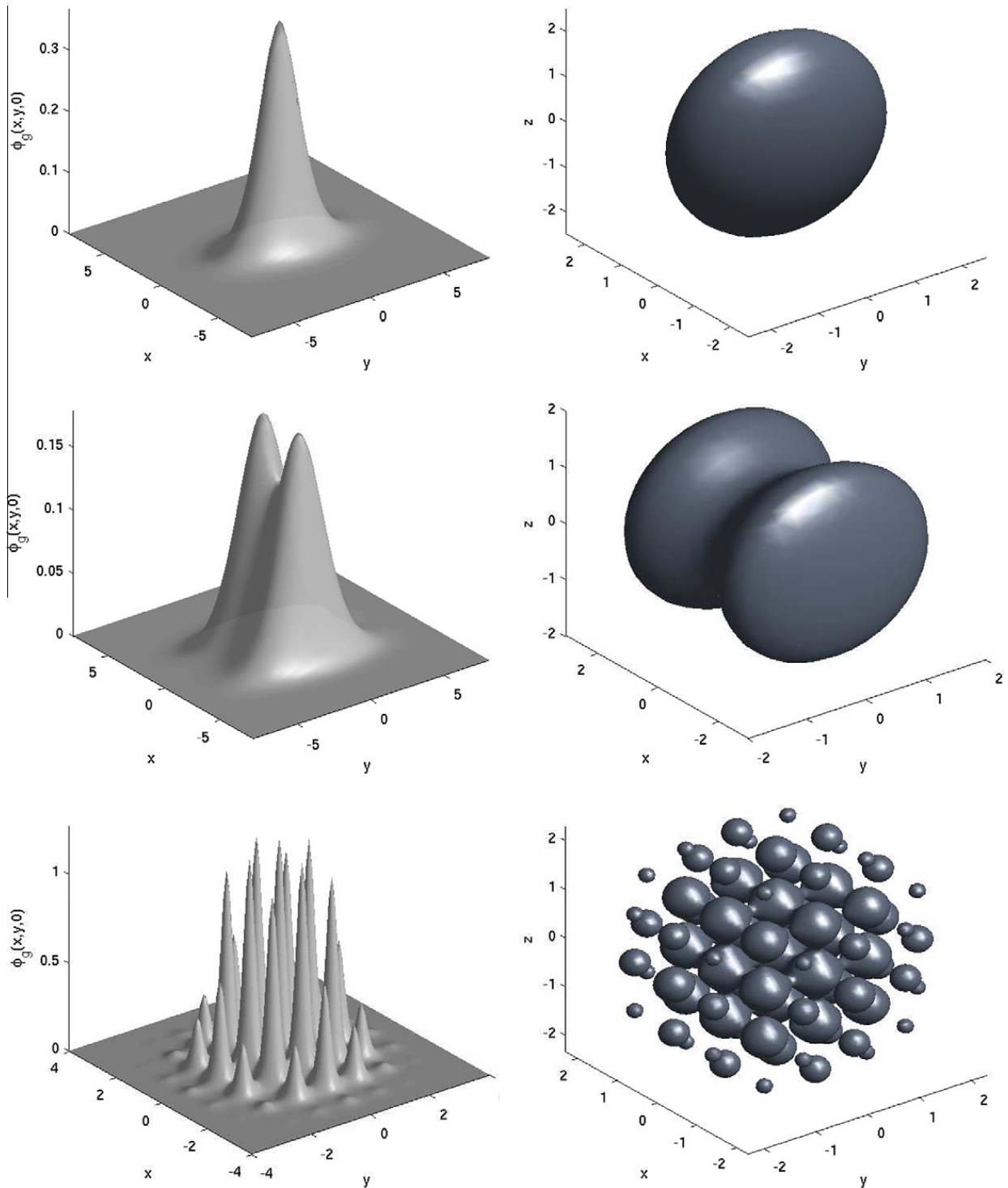


Fig. 3. Ground state solution ϕ_g in Example 2 for case (i) (top row), case (ii) (middle row) and case (iii) (bottom row): surface plots of $\phi_g(x,y,0)$ (left column); and isosurface plots of $|\phi_g| = 0.1$ (right column).

Example 2. Ground states of the RSP system with different non-spherically symmetric potentials in (1.7), i.e. we consider three cases: (i). $\beta = -10$ and $m = 1$ with a harmonic potential $V(x, y, z) = \frac{1}{32}(16x^2 + y^2 + z^2)$; (ii). $\beta = -10$ and $m = 1$ with a double-well potential $V(x, y, z) = \frac{1}{32}((4 - x^2)^2 + y^2 + z^2)$; and (iii). $\beta = 64$ and $m = 1$ with an optical lattice potential $V(x, y, z) = \frac{1}{2}(x^2 + y^2 + z^2) + 10(\sin^2(\pi x) + \sin^2(\pi y) + \sin^2(\pi z))$.

The problem is computed on a bounded domain $\Omega = [-8, 8]^3$ by using BESP-3D with mesh size $h_r = 1/8$ and time step $\Delta t = 0.01$. The initial data is taken as $\phi_0(x, y, z) = \frac{1}{(\pi/2)^{3/4}} e^{-(x^2+y^2+z^2)}$. Fig. 3 shows the surface plots of $\phi_g(x, y, 0)$ and isosurface plots of $|\phi_g| = 0.1$ for the above three cases. The results show that the BESP-3D method can compute the ground state very efficiently and accurately.

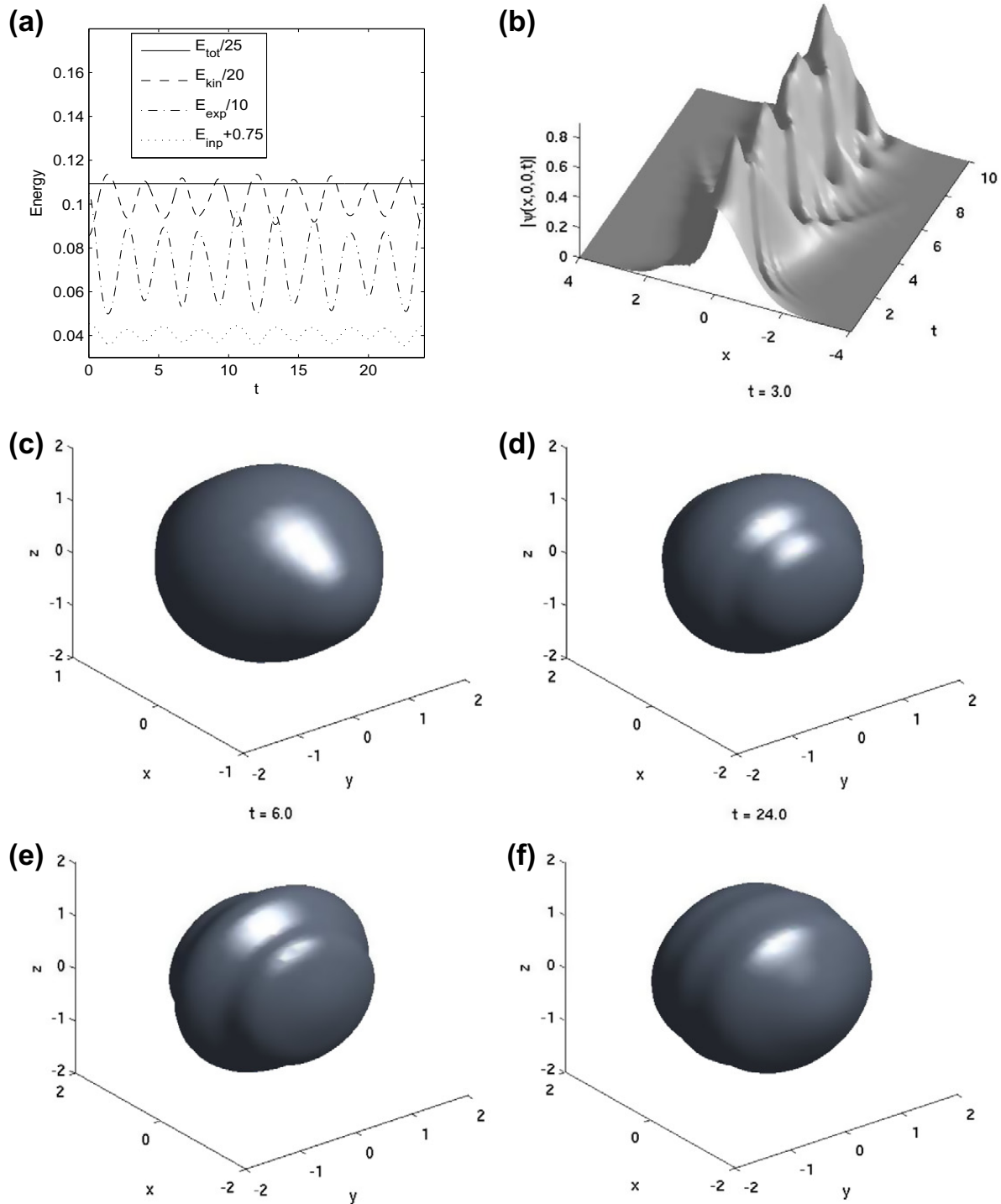


Fig. 4. Dynamics of the ground state when potential changes instantly from $V = \frac{1}{2}(x^2 + y^2 + z^2)$ to $V = \frac{1}{2}(4x^2 + y^2 + z^2)$, for $\beta = -1$ and $m = 1$ in Example 3: (a) evolution of various energies; (b) evolution of $|\psi(x,0,0,t)|$; (c)-(f) isosurface plots of $|\psi| = 0.1$ at different times.

5.3. Dynamics of the RSP system

Example 3. Dynamics of ground states under perturbation, i.e. we take initial condition as the ground states computed numerically by using the BESP-3D method. First, we study the evolution of the ground state under the potential $V = \frac{1}{2}(x^2 + y^2 + z^2)$ for $\beta = -1$ and $m = 1$, when the potential suddenly changes to $V = \frac{1}{2}(4x^2 + y^2 + z^2)$. We choose $\Omega = [-4, 4]^3$ with mesh size $h = 1/8$ and time step $\Delta t = 0.001$. Second, we look at the evolution of the ground state under a double-well potential $V(x, y, z) = \frac{1}{32}((4 - x^2)^2 + y^2 + z^2)$ for $\beta = -10$ and $m = 1$, when the potential suddenly changes to $V = \frac{1}{2}(x^2 + y^2 + z^2)$. In this case, we choose $\Omega = [-8, 8]^3$ with mesh size $h = 1/4$ and time step $\Delta t = 0.001$. Figs. 4 and 5 show the evolution of total energy, kinetic energy and external/internal potential energy, the evolutions of $\psi(x, 0, 0, t)$, and isosurface plots of $|\psi| = 0.1$ at different times for these two cases. In these two cases, the global-in-time existence of solution is observed. Also, our method conserves the total energy very well.

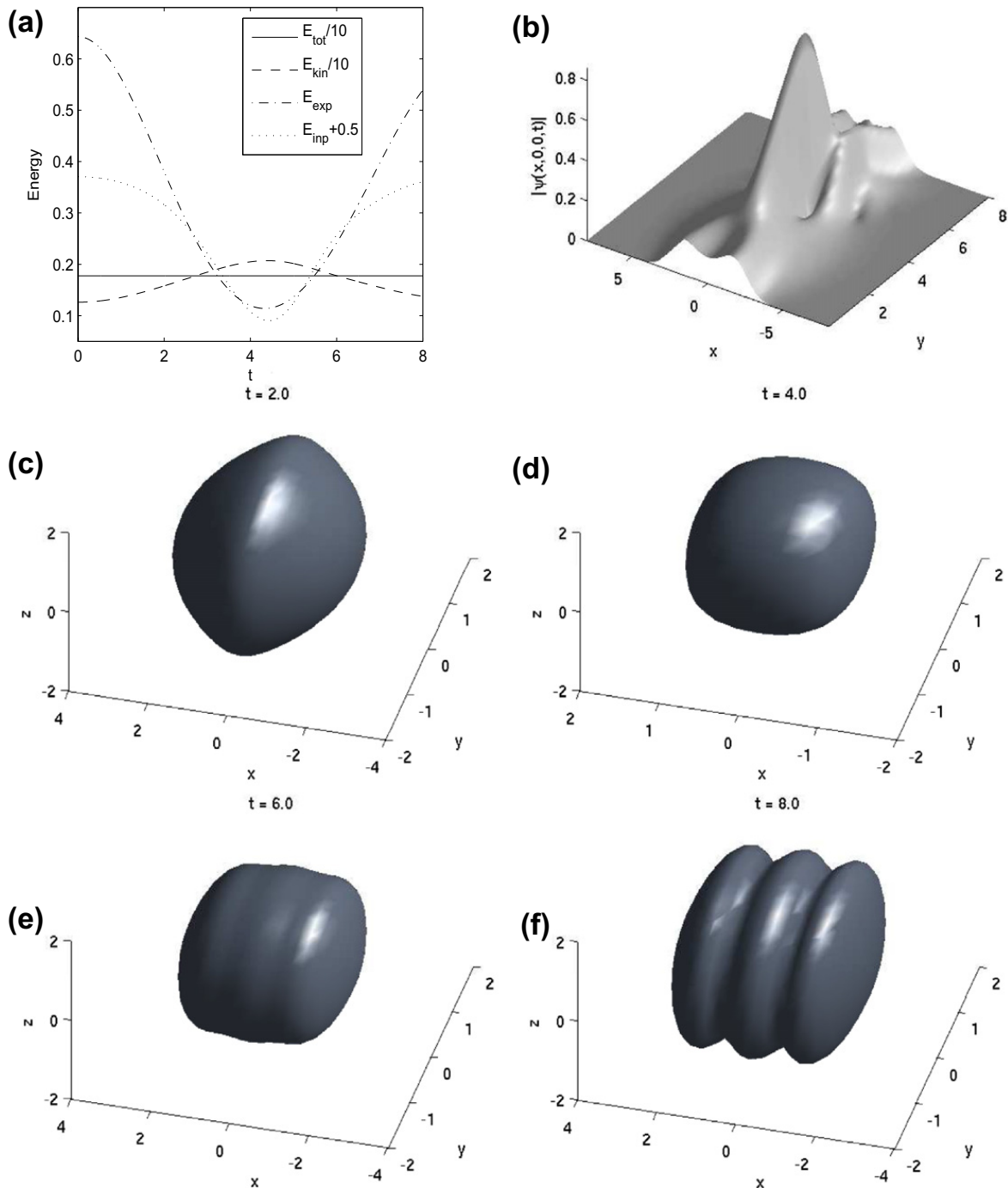


Fig. 5. Dynamics of the ground state when potential changes instantly from $V = \frac{1}{32}((4 - x^2)^2 + y^2 + z^2)$ to $V = \frac{1}{2}(4x^2 + y^2 + z^2)$, for $\beta = -10$ and $m = 1$ in Example 3: (a) evolution of various energies; (b) evolution of $|\psi(x, 0, 0, t)|$; (c)–(f) isosurface plots of $|\psi| = 0.1$ at different times.

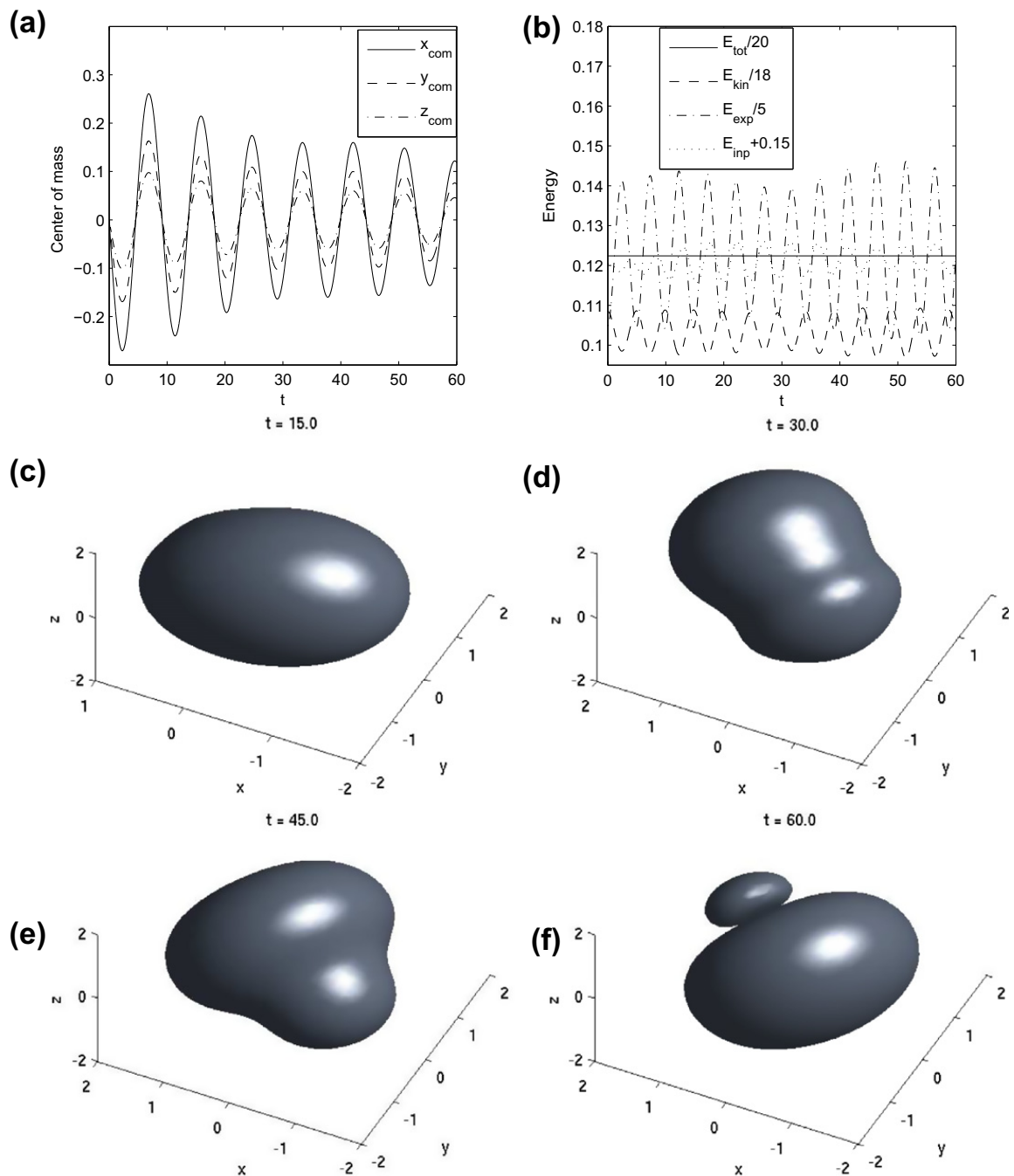


Fig. 6. Dynamics of the ground state enforced an instant movement in Example 3: (a) evolution of the center of mass ($x_{com}, y_{com}, z_{com}$); (b) evolution of various energies; (c)-(f) isosurface plots of $|\psi| = 0.1$ at different times. Here, $V = \frac{1}{2}(x^2 + y^2 + z^2)$, $m = 1$ and $\beta = -1$.

Next, we study the dynamics of the center of mass. Let ϕ_g be the ground state under the potential $V(x, y, z) = \frac{1}{2}(x^2 + y^2 + z^2)$ with $\beta = -1$ and $m = 1$, which is obtained numerically by the BSP-3D method on $[-4, 4]^3$ with mesh size $h = 1/8$. The initial condition is taken as

$$\psi_0(x, y, z) = \phi_g(x, y, z)e^{i(0.8x+0.5y+0.3z)},$$

and we apply the TSSP-3D method with mesh size $h = 1/4$ and time step $\Delta t = 0.001$. The center of mass, $(x_{com}, y_{com}, z_{com})$, is evaluated by

$$x_{com} = h_x h_y h_z \sum_{(i,j,k) \in \mathcal{T}_{JKL}} x_j |\psi_{jkl}^n|^2,$$

and similar for y_{com} and z_{com} .

Fig. 6 shows the evolution of each component of the center of mass, various energy as well as the isosurface plots of $|\psi| = 0.1$ at different times. An obvious damping phenomena in the center of mass is observed, and the damping frequencies in each component of the center of mass are identical even though the damping amplitudes differ.

Example 4. Wave-collision in the RSP system, i.e. we take the initial condition as

$$\psi_0 = \frac{1}{3(\pi/2)^{3/4}} e^{-(y^2+z^2)} \left(e^{i 0.8x - (x+2.5)^2} + 2e^{-i 0.5x - (x-2.5)^2} \right),$$

which is two Gaussian beams in x -axis with opposite moving directions, $V = \frac{1}{2}(x^2 + y^2 + z^2)$, $\beta = -1$ and $m = 1$. We apply the TSSP-3D method by choosing $\Omega = [-8, 8]^3$ with mesh size $h = 1/4$ and time step $\Delta t = 0.001$. Fig. 7 plots the evolution of various energies, the evolution of $|\psi(x, 0, 0, t)|$ and isosurface plots of $|\psi| = 0.05$ at different times. It shows that after a collision there is no significant new wave structure generated.

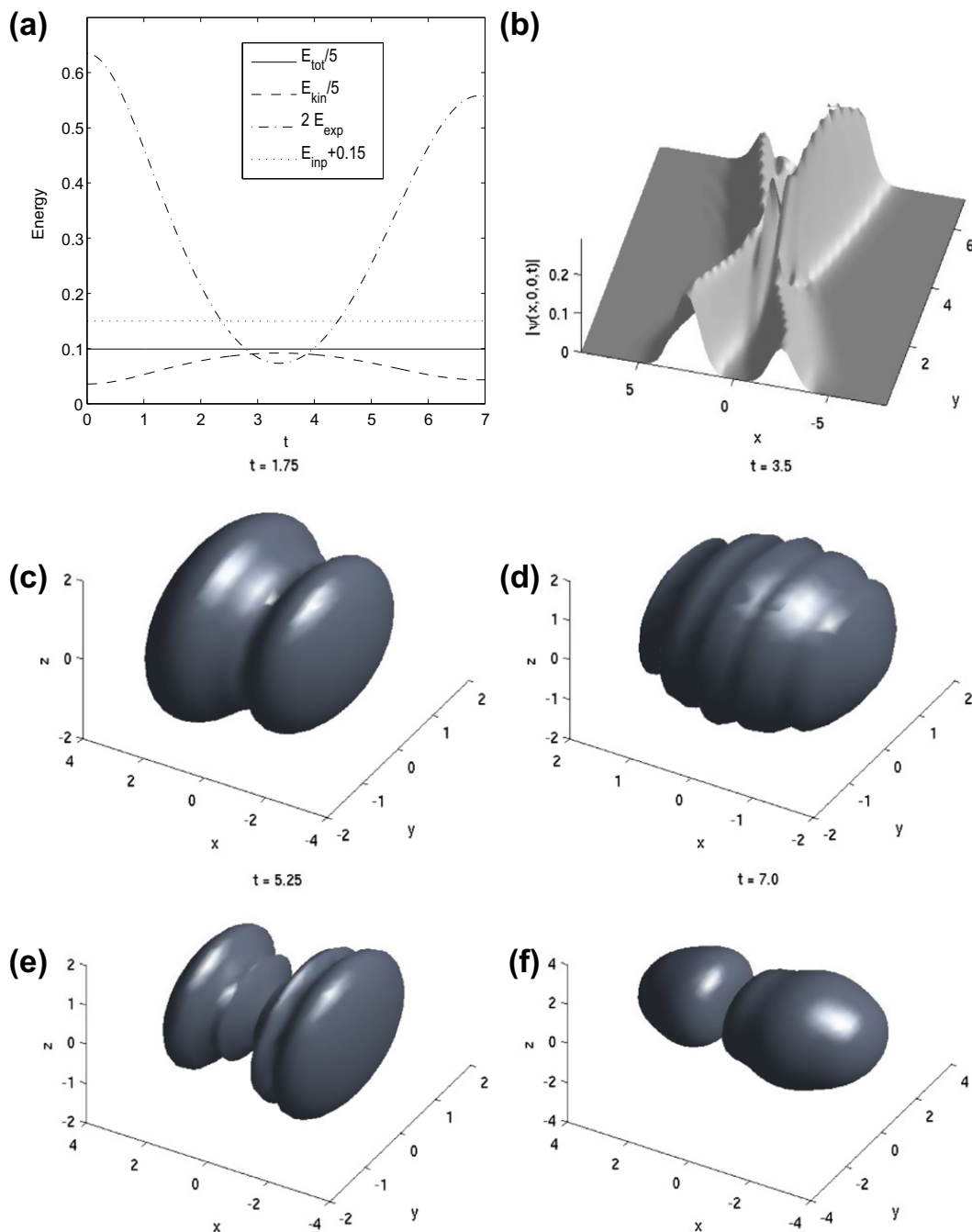


Fig. 7. Dynamics of two Gaussian beams with opposite moving directions: (a) evolution of various energies; (b) evolution of $|\psi(x, 0, 0, t)|$; (c)-(f) isosurface plots of $|\psi| = 0.05$ at different times.

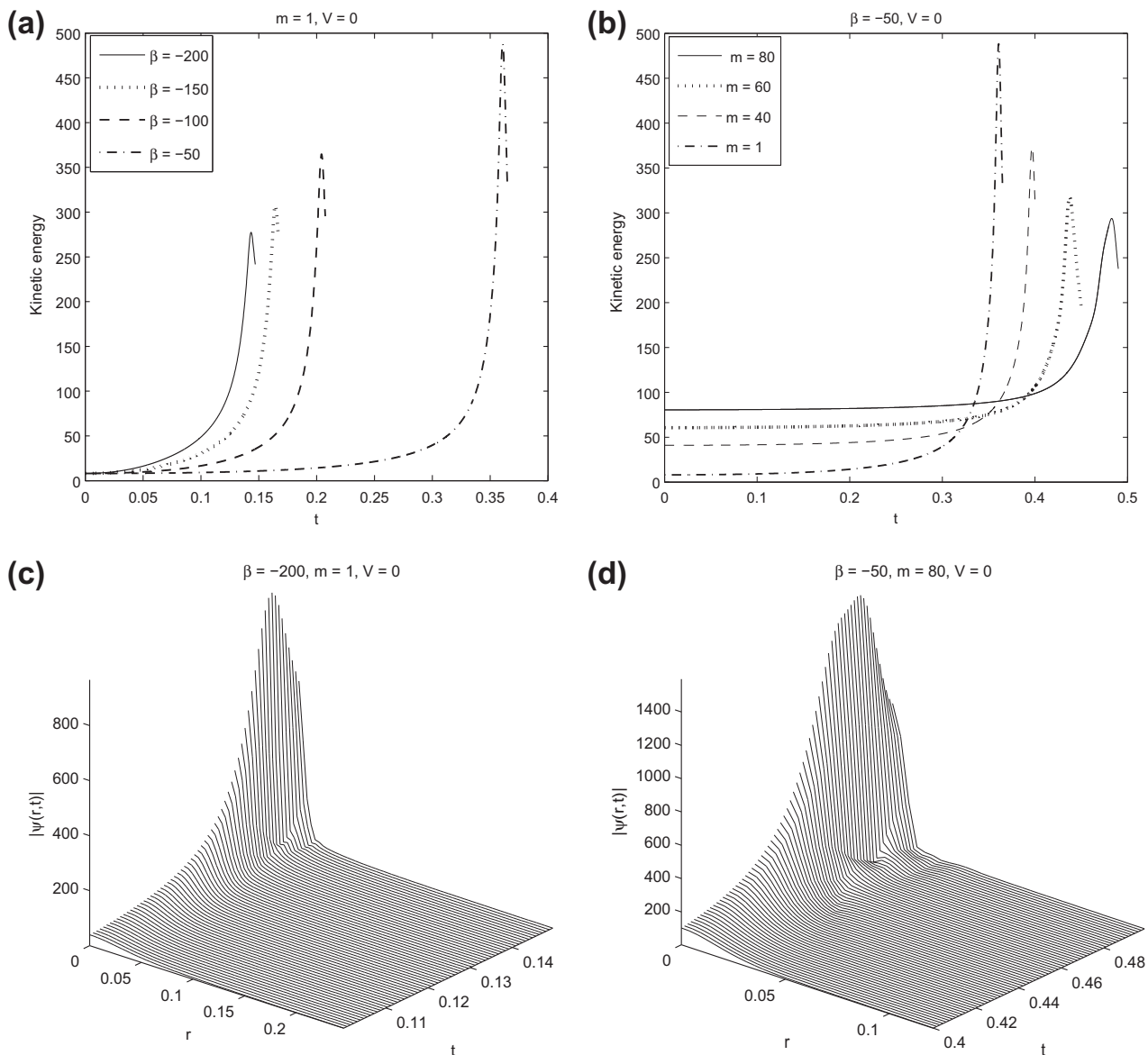


Fig. 8. Time evolution of kinetic energy in the blow-up cases when $V=0$ in Example 5: (a) for $\beta < 0$ and $m=1$, and (b) for $\beta = -50$ and different m ; and evolution of $|\psi(r,t)|$ close to the blow-up when $V(r)=0$: (c) for $\beta = -200$ and $m=1$, and (d) for $\beta = -50$ and $m=80$.

Example 5. Finite time blow-up in the RSP system, i.e. we investigate the change of the “gravitational collapse” time with respect to the particle mass as well as the total number of particles in boson stars without external potentials. The initial condition is taken as

$$\psi_0(r) = \frac{1}{(\pi/50)^{3/4}} e^{-25r^2},$$

and the TSSP-1D method is applied with $\Omega = [0,1], h_r = 1/256$ and $\Delta t = 0.0001$. The blow-up time is detected by looking at the evolution of the kinetic energy. First we fix the particle mass as $m=1$ and change β from -50 to -200 , and then choose $m=1, 40, 60$ and 80 , when $\beta = -50$. Fig. 8 shows the evolution of kinetic energy in these two settings, and depicts the evolution of $|\psi(r,t)|$ when $(\beta, m) = (-200, 1)$ and $(\beta, m) = (-50, 80)$. The results indicate a monotonic relation between the “gravitational collapse” time and both the particle mass and total particle number. More precisely, when either the total particle number increases or the particle mass decreases, the boson stars would collapse earlier.

6. Conclusion

We proposed efficient and accurate numerical methods for computing the ground state and dynamics of the nonlinear relativistic Hartree equation with general solutions, and respectively, spherically symmetric solutions. The main challenge

in the numerics lies in discretizing the pseudodifferential kinetic operator in three-dimensional space, which arises in special relativity. In general, the usual finite difference spatial discretizations cost much more memory load and/or computation time. In our methods, we applied the sine pseudospectral approach in spatial discretization, with which the kinetic operator is approximated by multiplying its eigenvalue in phase space. With this spatial discretization, a backward Euler sine pseudospectral (BESP) method was proposed to discretize a gradient flow with discrete normalization for computing the ground state. And, in particular, when the system has spherical symmetry, a BESP method was given based on a reduced one-dimensional problem. For dynamics, a time-splitting sine pseudospectral discretization was proposed for general and spherical-symmetric solutions. Numerical tests demonstrated that our methods are spectral accuracy in space, less demanding on memory and efficiently solvable. Applications of the methods in various setups were also reported. In the numerical results, some interesting properties of boson stars, which can be modeled by the relativistic Hartree equation as a mean-field limit, were observed. For example, the monotone of each component in the energy in ground states with respect to single particle mass, similar monotonic property in “gravitational collapse” time, and the damping phenomena in the dynamics of the center of mass were observed. In summary, we proposed efficient and accurate numerical methods for computing ground state and dynamics of the relativistic Hartree equation for boson stars, and applied them to study several properties of the system. Our results will pave a way to the future studies, especially on the ground states and mean field dynamics of boson stars.

Acknowledgements

This work was supported by Academic Research Fund of Ministry of Education of Singapore grant R-146-000-120-112. Part of this work was done when the authors were visiting the Isaac Newton Institute for Mathematical Sciences, University of Cambridge, in 2010.

References

- [1] A. Aftalion, Q. Du, Vortices in a rotating Bose–Einstein condensate: Critical angular velocities and energy diagrams in the Thomas–Fermi regime, *Phys. Rev. A* 64 (2001), article 063603.
- [2] G.L. Aki, P.A. Markowich, C. Sparber, Classical limit for semirelativistic Hartree systems, *J. Math. Phys.* 49 (2008) 102–110.
- [3] W. Bao, Y. Cai, H. Wang, Efficient numerical methods for computing ground states and dynamics of dipolar Bose–Einstein condensates, *J. Comput. Phys.* 229 (2010) 7874–7892.
- [4] W. Bao, I.-L. Chern, F.Y. Lim, Efficient and spectrally accurate numerical methods for computing ground and first excited states in Bose–Einstein condensates, *J. Comput. Phys.* 219 (2006) 836–854.
- [5] W. Bao, Q. Du, Computing the ground state solution of Bose–Einstein condensates by a normalized gradient flow, *SIAM J. Sci. Comput.* 25 (2004) 1674–1697.
- [6] W. Bao, S. Jin, P.A. Markowich, Time-splitting spectral approximations for the Schrödinger equation in the semiclassical regime, *J. Comput. Phys.* 175 (2002) 487–524.
- [7] W. Bao, S. Jin, P.A. Markowich, Numerical studies of time-splitting spectral discretizations of nonlinear Schrödinger equations in the semiclassical regime, *SIAM J. Sci. Comput.* 25 (2003) 27–64.
- [8] W. Bao, N.J. Mauser, H.P. Stimming, Effective one particle quantum dynamics of electrons: a numerical study of the Schrödinger–Poisson– X_z model, *Commun. Math. Sci.* 1 (2003) 809–828.
- [9] W. Bao, Y. Zhang, Dynamics of the ground state and central vortex states in Bose–Einstein condensation, *Math. Models Methods Appl. Sci.* 15 (2005) 1863–1896.
- [10] N. Ben Abdallah, P. Degond, P.A. Markowich, On a one-dimensional Schrödinger–Poisson scattering model, *ZAMP* 48 (1997) 135–155.
- [11] C. Besse, B. Bidégaray, S. Descombes, Order estimates in time of splitting methods for the nonlinear Schrödinger equation, *SIAM J. Numer. Anal.* 40 (2002) 26–40.
- [12] M.L. Chiofalo, S. Succi, M.P. Tosi, Ground state of trapped interacting Bose–Einstein condensates by an explicit imaginary-time algorithm, *Phys. Rev. E* 62 (2000) 7438–7444.
- [13] Y. Cho, T. Ozawa, On the semirelativistic Hartree-type equation, *SIAM J. Math. Anal.* 38 (2006) 1060–1074.
- [14] K.T.R. Davies, H. Flocard, S. Krieger, M.S. Weiss, Application of the imaginary time step method to the solution of the static Hartree–Fock problem, *Nucl. Phys. A* 342 (1980) 111–123.
- [15] M. Edwards, K. Burnett, Numerical solution of the nonlinear Schrödinger equation for small samples of trapped neutral atoms, *Phys. Rev. A* 51 (1995) 1382–1386.
- [16] M. Ehrhardt, A. Zisowsky, Fast calculation of energy and mass preserving solutions of Schrödinger–Poisson systems on unbounded domains, *J. Comput. Appl. Math.* 187 (2006) 1–28.
- [17] A. Elgart, B. Schlein, Mean field dynamics of Boson stars, *Commun. Pure Appl. Math.* 60 (2007) 500–545.
- [18] B. Fornberg, *A Practical Guide to Pseudospectral Methods*, Cambridge University Press, Cambridge, 1998.
- [19] J. Fröhlich, B.L. Jonsson, E. Lenzmann, Effective dynamics for boson stars, *Nonlinearity* 20 (2007) 1031–1075.
- [20] J. Fröhlich, E. Lenzmann, Blowup for nonlinear wave equations describing boson stars, *Commun. Pure Appl. Math.* 60 (2007) 1691–1705.
- [21] A. Gammal, T. Frederico, L. Tomio, Improved numerical approach for the time-independent Gross–Pitaevskii nonlinear Schrödinger equation, *Phys. Rev. E* 60 (1999) 2421–2424.
- [22] D. Gottlieb, S.A. Orszag, *Numerical Analysis of Spectral Methods: Theory and Applications*, Society for Industrial and Applied Mathematics, Philadelphia, 1993.
- [23] R. Harrison, I.M. Moroz, K.P. Tod, A numerical study of Schrödinger–Newton equations, *Nonlinearity* 16 (2003) 101–122.
- [24] J.S. Hesthaven, S. Gottlieb, D. Gottlieb, *Spectral Methods for Time-Dependent Problems*, Cambridge University Press, Cambridge, New York, 2007.
- [25] H. Holden, C.X. Karlsen, K.-A. Lie, N.H. Risebro, *Splitting Methods for Partial Differential Equations with Rough Solutions: Analysis and MATLAB programs*, European Mathematical Society, Zürich, 2010.
- [26] L. Lehtovaara, J. Toivanen, J. Eloranta, Solution of time-independent Schrödinger equation by the imaginary time propagation method, *J. Comput. Phys.* 221 (2007) 148–157.
- [27] E. Lenzmann, Well-posedness for semi-relativistic Hartree equations of critical type, *Math. Phys. Anal. Geom.* 10 (2007) 43–64.
- [28] E. Lenzmann, Uniqueness of ground states for pseudo-relativistic Hartree equations, *Anal. PDE* 1 (2009) 1–30.
- [29] E.H. Lieb, H. Yau, The Chandrasekhar theory of stellar collapse as the limit of quantum mechanics, *Commun. Math. Phys.* 112 (1987) 147–174.
- [30] C. Lubich, On splitting methods for Schrödinger–Poisson and cubic nonlinear Schrödinger equations, *Math. Comput.* 77 (2008) 2141–2153.
- [31] G.I. Marchuk, Splitting and alternating direction methods, *Handbook of Numerical Analysis*, vol. I, North-Holland, Amsterdam, 1990. pp. 197–462.

- [32] V.S. Popov, Imaginary-time method in quantum mechanics and field theory, *Phys. At. Nucl.* 68 (2005) 686–708.
- [33] J. Shen, T. Tang, *Spectral and High-Order Methods with Applications*, Science Press, Beijing, 2006.
- [34] G. Strang, On the construction and comparison of difference schemes, *SIAM J. Numer. Anal.* 5 (1968) 505–517.
- [35] M. Thalhammer, M. Caliri, C. Neuhauser, High-order time-splitting Hermite and Fourier spectral methods, *J. Comput. Phys.* 228 (2009) 822–832.
- [36] Y. Zhang, X. Dong, On the computation of ground state and dynamics of Schrödinger–Poisson–Slater system, *J. Comput. Phys.* 230 (2011) 2660–2676.